超新星内部でのニュートリノ振動

2017.3.4 第三回超新星ニュートリノ研究会@東北大
Hideyuki Suzuki, Tokyo Univ. of Science

超新星コア ($T\sim 10\mathrm{MeV}, \rho \gtrsim 10^{14}\mathrm{g/cm}^3$)

- $\tau_{\mathrm{weak}} \ll \tau_{\mathrm{dyn}}$ ニュートリノの閉じ込め
  $\Rightarrow$ 熱平衡・化学平衡 $n_\nu \sim n_\gamma \sim n_{\mathrm{e}}$

  $$\tau_{\mathrm{weak}} \sim \frac{1}{\sigma_{\mathrm{weak}} n_{\mathrm{target}} v_{\mathrm{relative}}} \sim 3\cdot 10^{-9}\mathrm{sec}\left(\frac{T}{10\mathrm{MeV}}\right)^{-2}\left(\frac{\rho}{3\cdot 10^{14}\mathrm{g/cm}^3}\right)^{-1}$$

  $$\sigma_{\mathrm{weak}} \sim G_F^2 E_\nu^2 \sim G_F^2 (3T)^2,\ n_{\mathrm{target}} \sim \frac{\rho}{m_u},\ v_{\mathrm{relative}} \sim c$$

  $$\tau_{\mathrm{dyn}} \sim \frac{1}{\sqrt{G\rho}} \sim 0.2\mathrm{msec}\left(\frac{\rho}{3\cdot 10^{14}\mathrm{g/cm}^3}\right)^{-1/2}$$

- 平均自由行程 $\lambda_\nu \sim \tau_{\mathrm{weak}} c \sim O(10^2)\mathrm{cm} \gg \lambda_\gamma, \lambda_{\mathrm{e}}, \lambda_N$
  $\Rightarrow$ ニュートリノがエネルギーを輸送し、コアの進化を駆動
  $\Rightarrow$ ニュートリノによって超新星コア (ニュートリノ球：neutrinosphere) が観測できる。
  $\tau_{\mathrm{diff}} = \frac{3R^2}{c\lambda_\nu} \sim O(1) - O(10)\mathrm{sec}$

ニュートリノ源としての特徴

- 3 世代 6 種類 ($\nu_{\rm e}$,$\bar{\nu}_{\rm e}$,ν_μ,$\bar{\nu}_\mu$,ν_τ,$\bar{\nu}_\tau$) のニュートリノ源
- $T < O(100{\rm MeV}) = m_\mu \Rightarrow n_{\rm e^-} \gg n_\mu, n_\tau$: $\nu_x \equiv \nu_\mu, \bar{\nu}_\mu, \nu_\tau, \bar{\nu}_\tau$
- 強度: $\int L_\nu dt \sim O(10^{53}){\rm erg} \sim 10^4 L_{\nu\odot}\tau_\odot \sim 10^2 L_{\gamma\odot}\tau_\odot$
- 時間: $\tau \sim O(10){\rm sec}$
- 基線長: $d > O(1){\rm pc} \sim O(10^{18}){\rm cm}$
- 光度曲線，エネルギースペクトルの違い
  平均エネルギー ($O(10){\rm MeV}$) の階層性

$$
\begin{array}{ccccc}
\sigma_{\nu_{\rm e}} & > & \sigma_{\bar{\nu}_{\rm e}} & > & \sigma_{\nu_x} \\
R_{\nu_{\rm e}} & > & R_{\bar{\nu}_{\rm e}} & > & R_{\nu_x} \\
T_{\nu_{\rm e}} & < & T_{\bar{\nu}_{\rm e}} & < & T_{\nu_x} \\
\langle\omega_{\nu_{\rm e}}\rangle & < & \langle\omega_{\bar{\nu}_{\rm e}}\rangle & < & \langle\omega_{\nu_x}\rangle
\end{array}
$$

- 高密度物質を通過 ($\rho = 0 \sim 10^{15}{\rm g/cm}^3$): 高密度 MSW 共鳴、集団振動
- 低頻度

ニュートリノ反応

$T \lesssim 100\mathrm{MeV}$, $\rho \lesssim 10^{15}\mathrm{g/cm}^3$: $\mu^{\pm}, \tau^{\pm}$ は無視することが多い

$\nu \equiv (\nu_\mathrm{e}, \bar{\nu}_\mathrm{e}, \nu_\mu, \bar{\nu}_\mu, \nu_\tau, \bar{\nu}_\tau)$, $\nu_\mathrm{e}\,\bar{\nu}_\mathrm{e}$ 以外を ν_μ または $\nu_x = \frac{1}{4}(\nu_\mu + \bar{\nu}_\mu + \nu_\tau + \bar{\nu}_\tau)$ と記す

放出、吸収

$\mathrm{e}^-\mathrm{p} \longleftrightarrow \nu_\mathrm{e}\mathrm{n}$

$\mathrm{e}^+\mathrm{n} \longleftrightarrow \bar{\nu}_\mathrm{e}\mathrm{p}$

$\mathrm{e}^- A(N,Z) \longleftrightarrow \nu_\mathrm{e} A'(N+1, Z-1)$

$\mathrm{e}^-\mathrm{e}^+ \longleftrightarrow \nu\bar{\nu}$

$\mathrm{plasmon} \longleftrightarrow \nu\bar{\nu}$

$\mathrm{NN}' \longleftrightarrow \mathrm{NN}'\nu\bar{\nu}$ (核子制動輻射)

$\mathrm{Nn} \longleftrightarrow \mathrm{Np}\ell^-\bar{\nu}_\ell$, $\mathrm{Np}\ell^- \longleftrightarrow \mathrm{Nn}\nu_\ell$ (modified URCA)

散乱

$\nu\mathrm{A} \longrightarrow \nu\mathrm{A}$

$\nu\mathrm{N} \longrightarrow \nu\mathrm{N}$

$\nu\ell \longrightarrow \nu\ell$

$\nu\nu' \longrightarrow \nu\nu'$

$\mathrm{NN}\nu \longrightarrow \mathrm{NN}\nu$

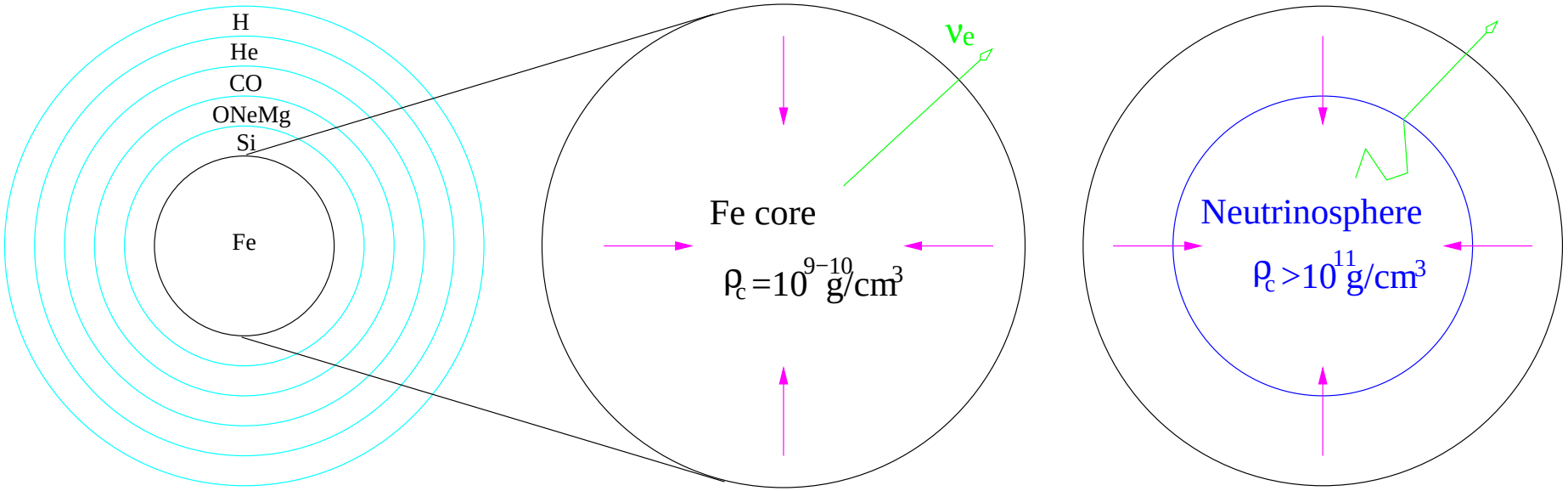

ν trapping ($\rho > 10^{10} - 10^{12}\mathrm{g/cm}^3$)

ν_e from $\mathrm{e}^- \mathrm{A} \longrightarrow \nu_\mathrm{e} \mathrm{A}'$ and $\mathrm{e}^- \mathrm{p} \longrightarrow \nu_\mathrm{e} \mathrm{n}$

main opacity source: coherent scattering $\nu_\mathrm{e} \mathrm{A} \longrightarrow \nu_\mathrm{e} \mathrm{A}$

cross section $\sigma \propto A^2 \omega_\nu^2$: $\lambda_{\nu \mathrm{A}} < \lambda_{\nu \mathrm{N}}$

(ν wave length $\frac{\hbar c}{E_\nu} \sim 20\mathrm{fm}(\frac{E_\nu}{10\mathrm{MeV}})^{-1} \gg$ nuclear size $1.2A^{\frac{1}{3}}\mathrm{fm} \sim 5\mathrm{fm}(\frac{A}{56})^{\frac{1}{3}}$)

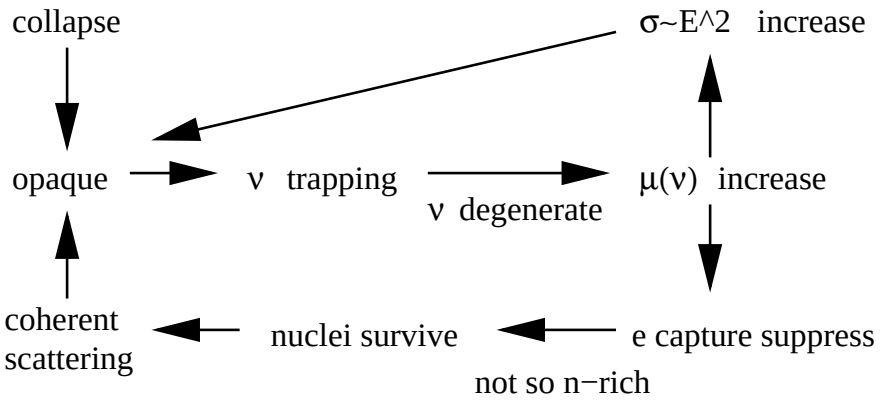

Positive feedback (Sato 1975)

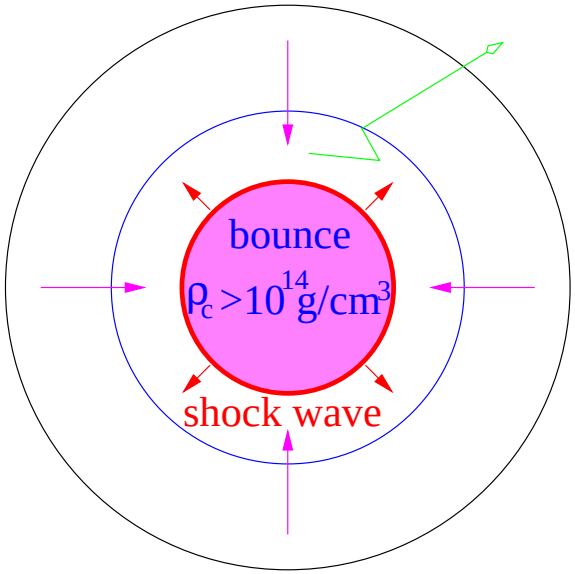

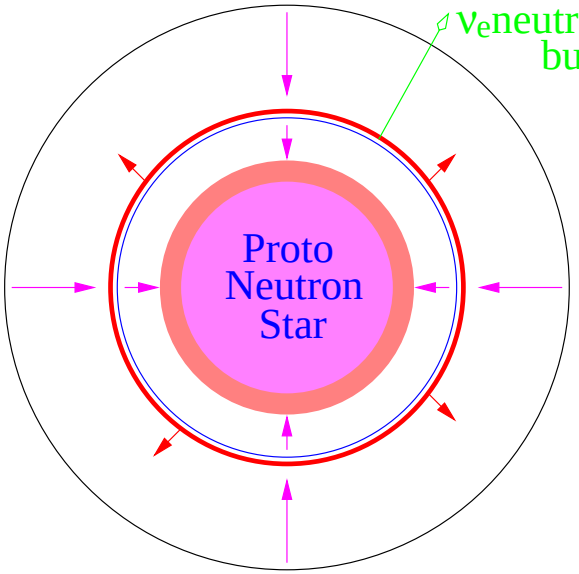

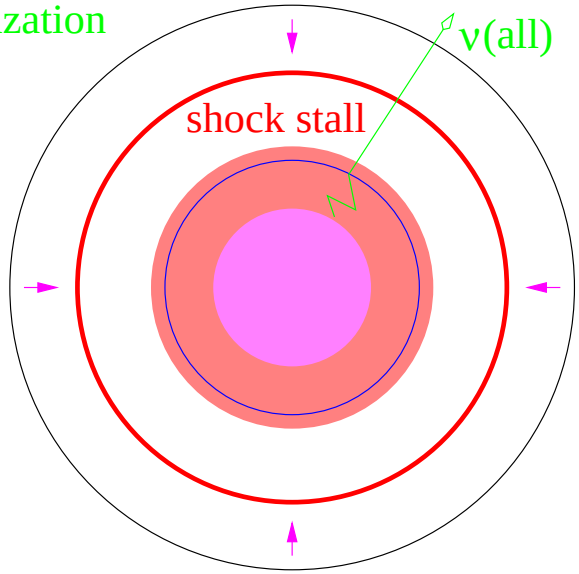

τ(collapse)~O(10−100)ms τ (neutronization burst)<O(10)ms t(stall)=O(100ms)

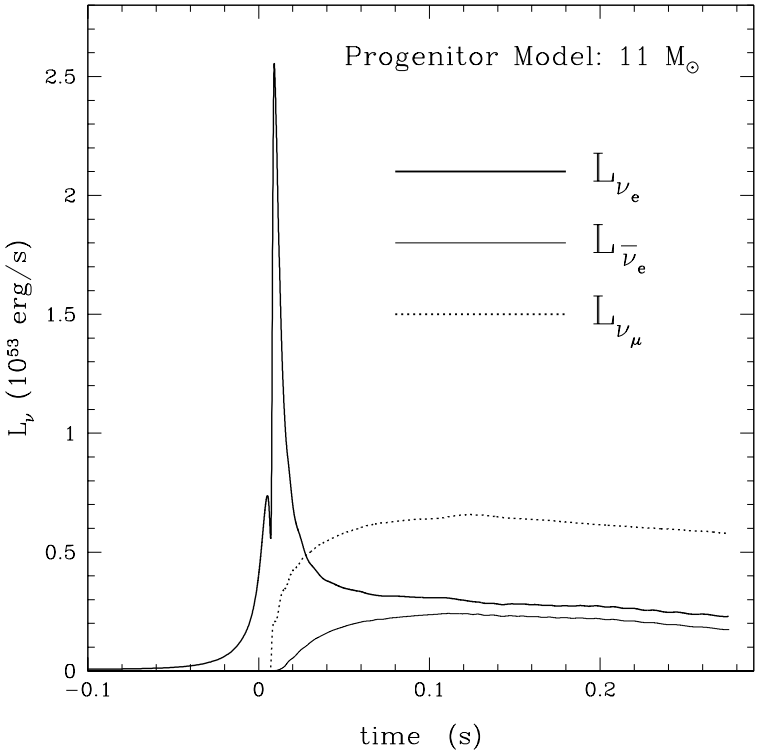

Neutronization burst. Thompson *et al.*, ApJ 592 (2003) 434
Fig.6 (failed explosion)

Shocked region
$A \to np, \quad e^- p \to n\nu_e$
$\sigma(e^- A \to \nu_e A') < \sigma(e^- p \to \nu_e n)$

dip around the bounce:
rapid compression $\to R_\nu \searrow$, redshift

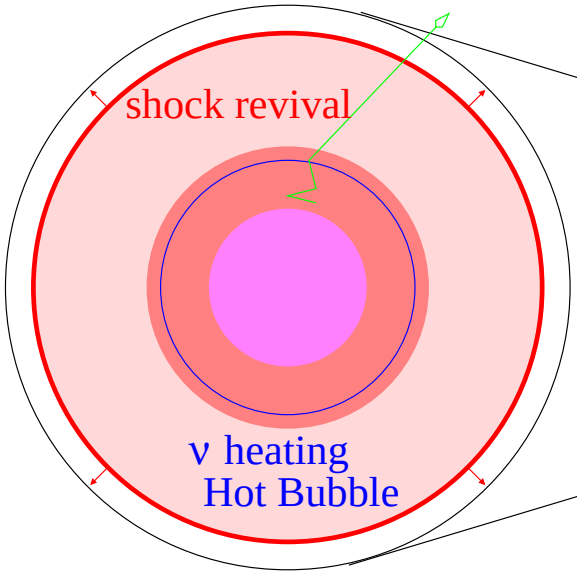

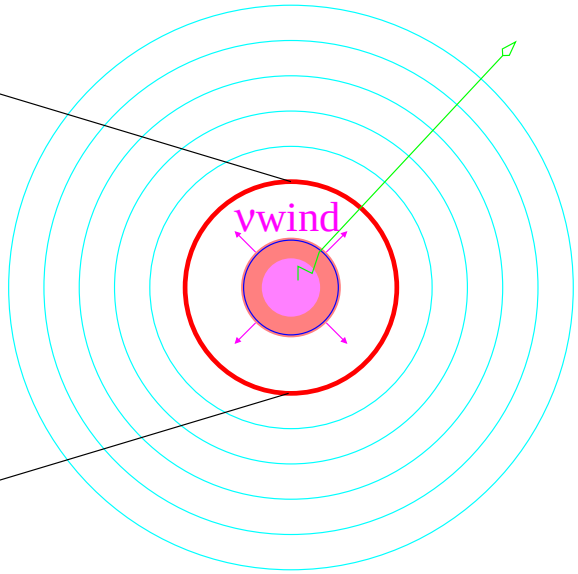

t(core exp.)=O(1)s

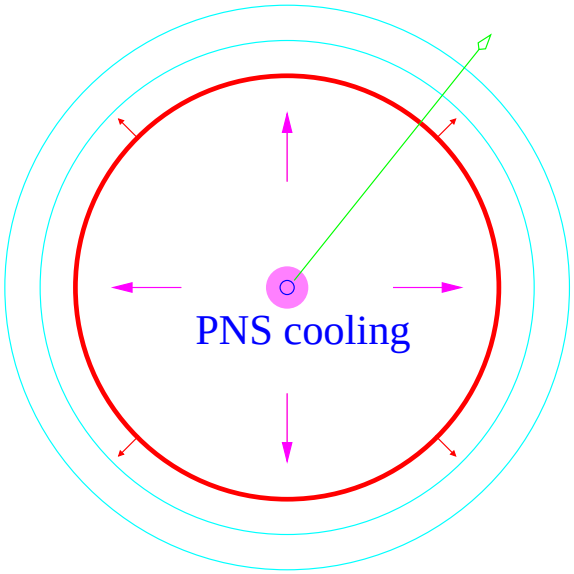

τ(PNS cooling)=O(10)s

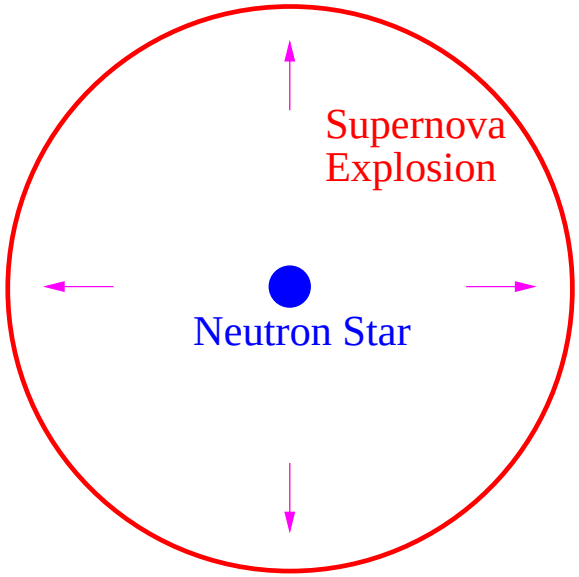

t(SNE)=hours−day

SN1987A

Crab nebula (remnant of SN1054)

Classical Simulations

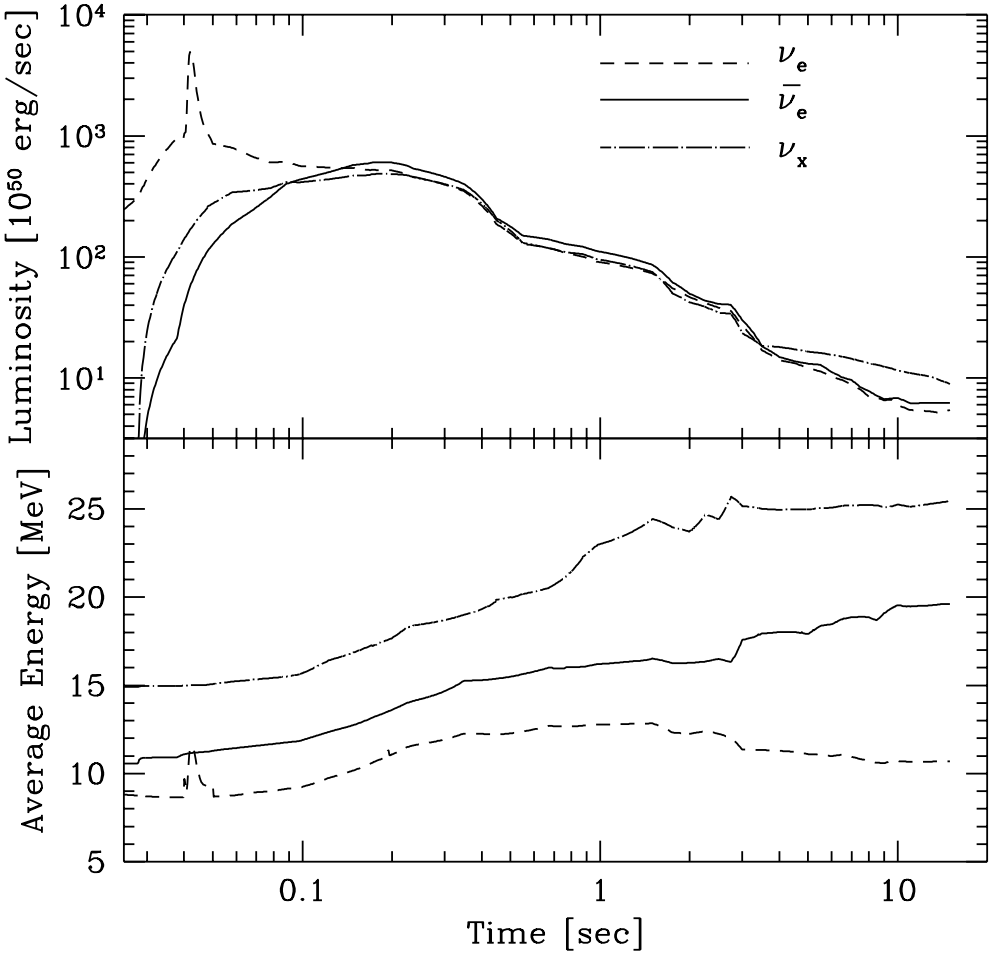

Totani *et al.*, 1998

early phase: hierarchy of average energy
late phase: n-rich matter interacts $\bar{\nu}_{\rm e}$ and ν_x almost equally. degeneracy prohibits $\nu_{\rm e}$ interactions, too.

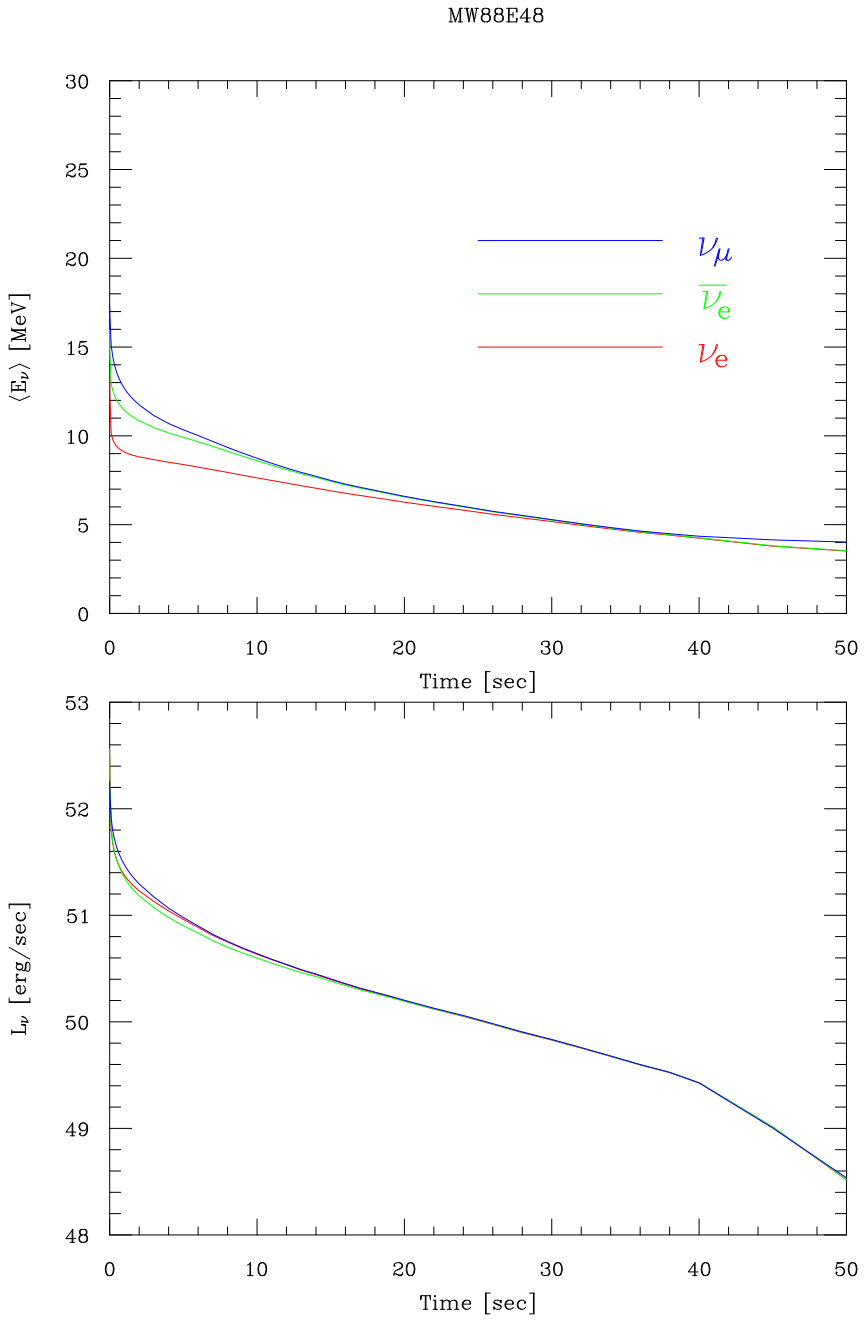

neutrinos from protoneutron star cooling phase

(Suzuki 2002)

Energetics

- $\Delta E_G = \left(\frac{GM_{\rm core}^2}{R_{\rm Fe\ core}} - \frac{GM_{\rm core}^2}{R_{\rm NS}} \right) \sim O(10^{53}){\rm erg}$
- $E_{\rm kin}({\rm obs.}) \sim O(10^{51}){\rm erg},\ E_{\rm rad}({\rm obs.}) \sim O(10^{49}){\rm erg}$
- 残り $O(10^{53}){\rm erg} \sim E_\nu$ cf. $E_\nu({\rm SNIa}) < 10^{49}{\rm erg}$

すべての陽子が中性子に変ったとしても放出される $\nu_{\rm e}$ は、

$$26 \frac{M_{\rm Fe\ core}}{m_{\rm Fe}} \langle E_{\nu_{\rm e}} \rangle \sim 1.2 \cdot 10^{52}{\rm erg} \frac{M_{\rm Fe\ core}}{1.4 M_\odot} \frac{\langle E_{\nu_{\rm e}} \rangle}{10{\rm MeV}} \sim O(0.1) \times E_{\nu\ {\rm tot}}$$

$\Longrightarrow$ thermal ν $\gg$ 電子捕獲に伴う $\nu_{\rm e}$ $\Longrightarrow$ $\nu_{\rm e}$, $\bar{\nu}_{\rm e}$, ν_xがほぼ同等に寄与

Modern Simulations

Light ONeMg core + CO shell($1.38M_\odot$): weak explosion ($O(10^{50})$erg)

(Progenitor: Nomoto 8-10$M_\odot$)

ν-heating + nuclear reaction $\Rightarrow$ weak explosion

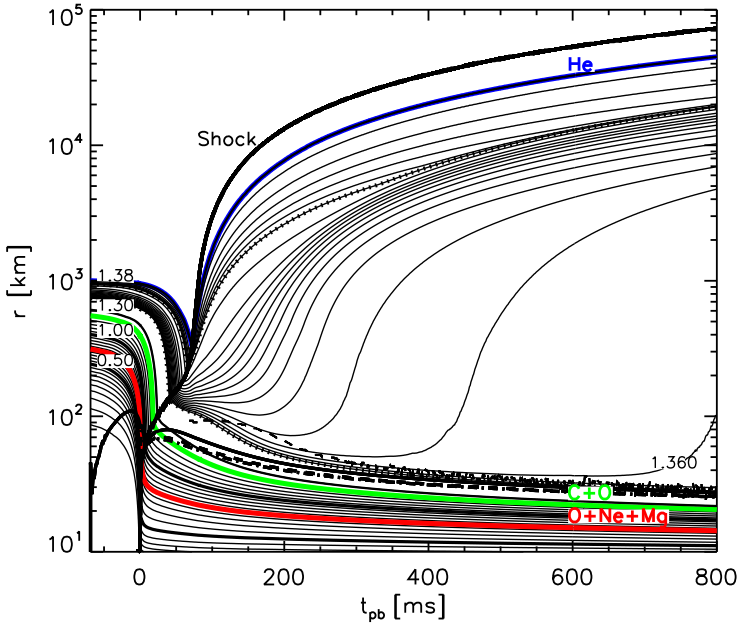

Fig. 1. Mass trajectories for the simulation with the W&H EoS as a function of post-bounce time (t_{pb}). Also plotted: shock position (thick solid line starting at time zero and rising to the upper right corner), gain radius (thin dashed line), and neutrinospheres (ν_e: thick solid; $\bar{\nu}_e$: thick dashed; ν_μ, $\bar{\nu}_\mu$, ν_τ, $\bar{\nu}_\tau$: thick dash-dotted). In addition, the composition interfaces are plotted with different bold, labelled lines: the inner boundaries of the O-Ne-Mg layer at ~0.77 $M_\odot$, of the C-O layer at ~1.26 $M_\odot$, and of the He layer at 1.3769 $M_\odot$. The two dotted lines represent the mass shells where the mass spacing between the plotted trajectories changes. An equidistant spacing of $5\times10^{-2}M_\odot$ was chosen up to $1.3579M_\odot$, between that value and $1.3765M_\odot$ it was $1.3\times10^{-3}M_\odot$, and $8\times10^{-5}M_\odot$ outside.

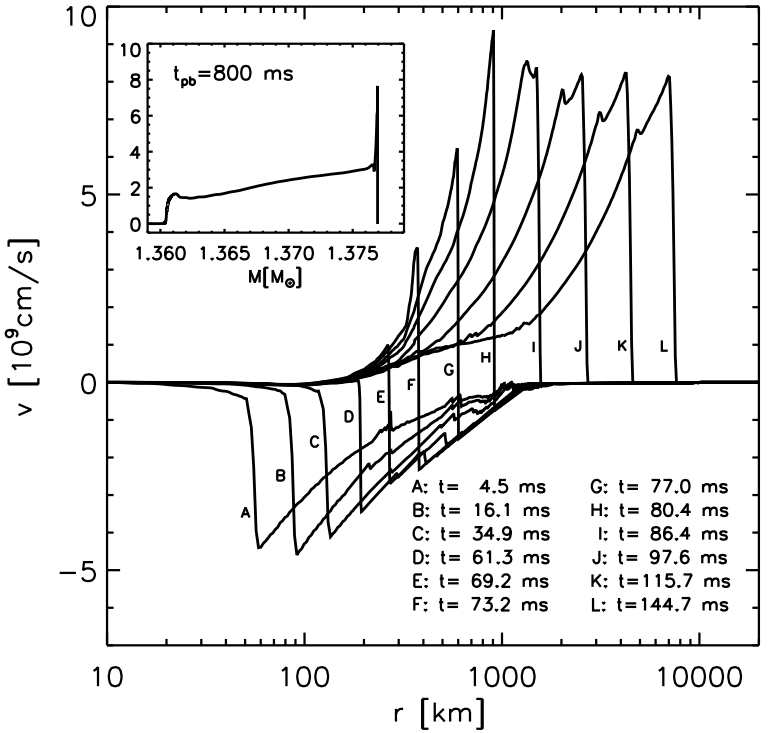

Fig. 3. Velocity profiles as functions of radius for different post-bounce times for the simulation with the W&H EoS. The insert shows the velocity profile vs. enclosed mass at the end of our simulation.

Kitaura *et al.*, AAp 450(2006)345

(Mezzacappa'07: $11.2M_\odot$model explodes, too)

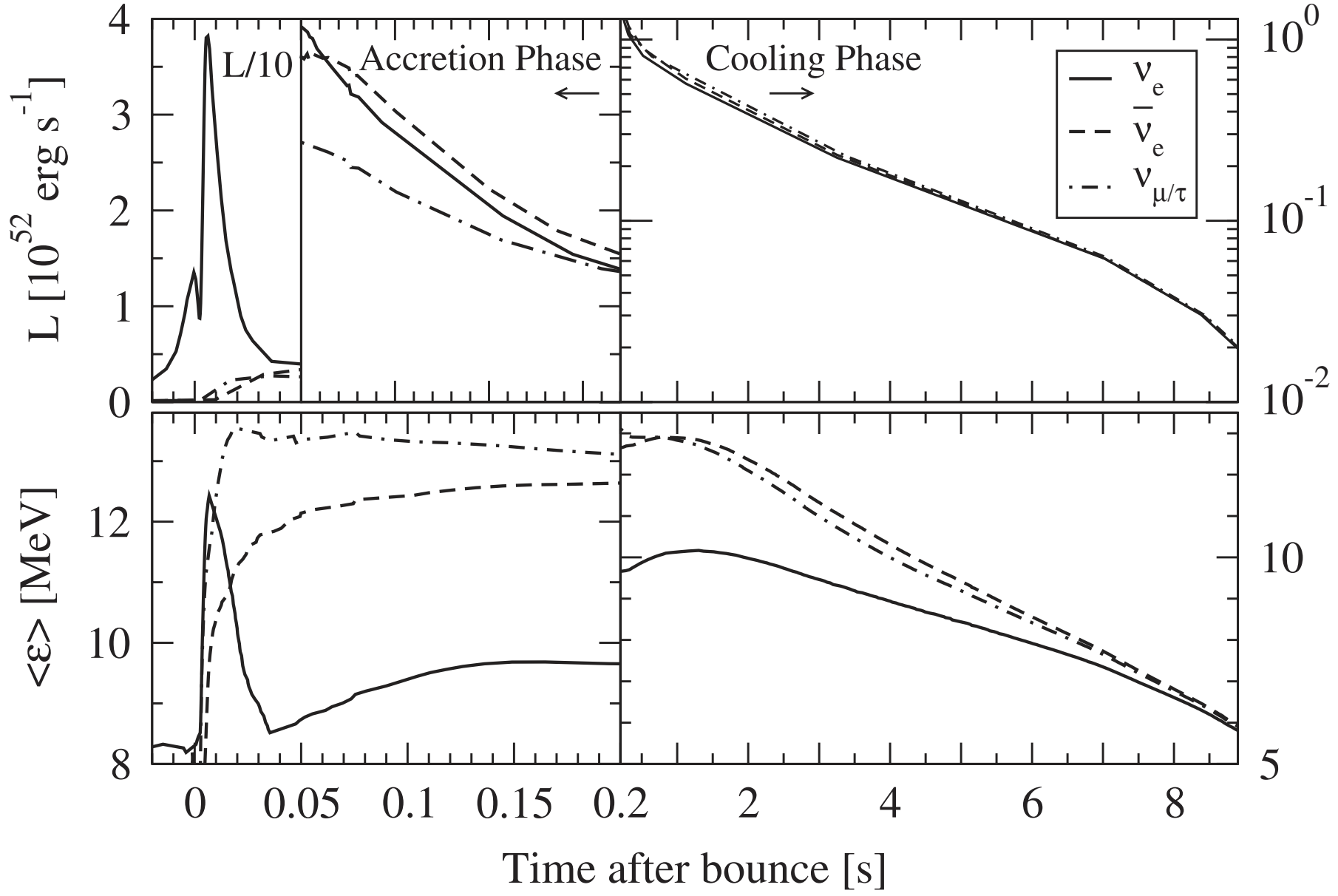

Neutrino luminosities and average energies at infinity for $8.8 M_\odot$ progenitor.
L. Hüdepohl *et al.*, PRL104 (2010) 251101

Modern simulations with GR 1D Boltzmann ν-transfer

canonical models: no explosion

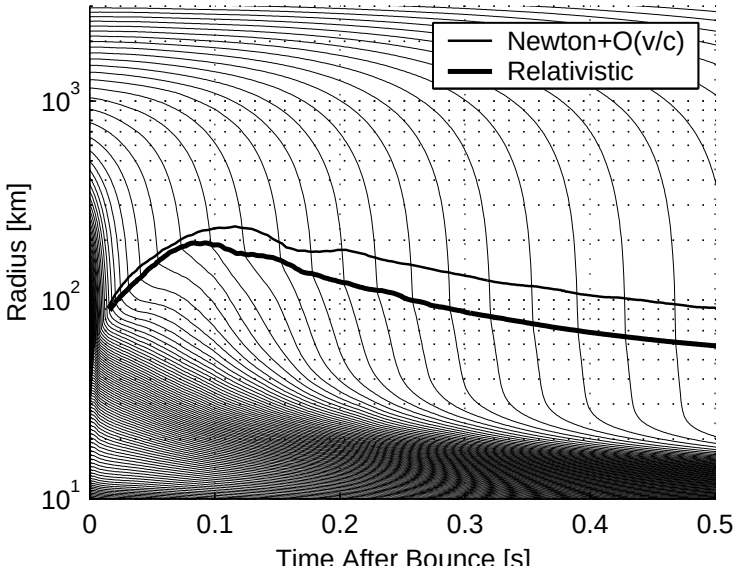

NH $13M_\odot$, GR Boltzman, LS EOS+Si burning Liebendörfer *et al.*, Phys.Rev. D63 (2001) 103004 (astro-ph/0006418 v2) Fig.6

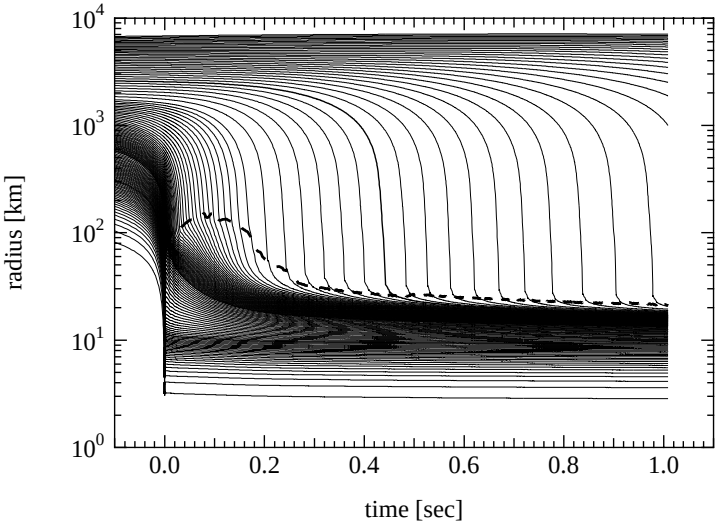

$15M_\odot$, Shen EOS, Sumiyoshi *et al.*, 2005.

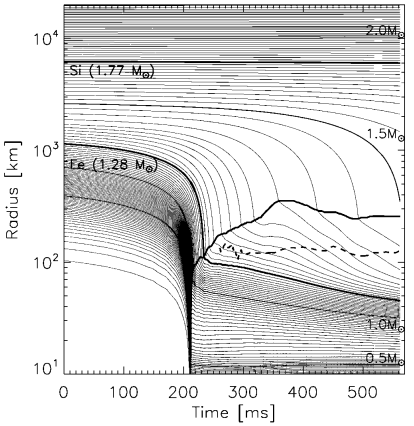

FIG. 1.—Trajectories of selected mass shells vs. time from the start of the simulation. The shells are equidistantly spaced in steps of 0.02 $M_\odot$, and the trajectories of the outer boundaries of the iron core (at 1.28 $M_\odot$) and of the silicon shell (at 1.77 $M_\odot$) are indicated by thick lines. The shock is formed at 211 ms. Its position is also marked by a thick line. The dashed curve shows the position of the gain radius.

WW $15M_\odot$, $M_{\rm Fe} = 1.28M_\odot$, NR Boltzmann (tangent-ray method), only $\nu_{\rm e}$,$\bar{\nu}_{\rm e}$, without $e^- e^+ \leftrightarrow \nu\bar{\nu}$, LS EOS, Rampp *et al.*, ApJ 539 (2000) L33 Fig.1

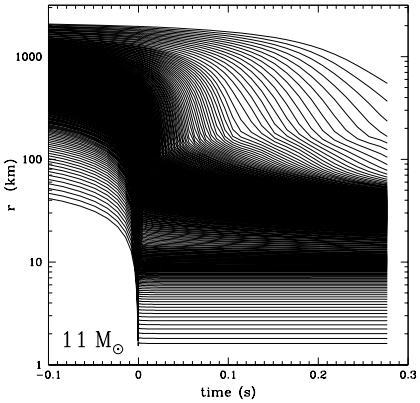

FIG. 5.—Radial position (in km) of selected mass shells as a function of time in our fiducial 11 $M_\odot$ model.

NR 1D Boltzmann ν-transfer, Thompson *et al.*, ApJ 592 (2003) 434 Fig.5

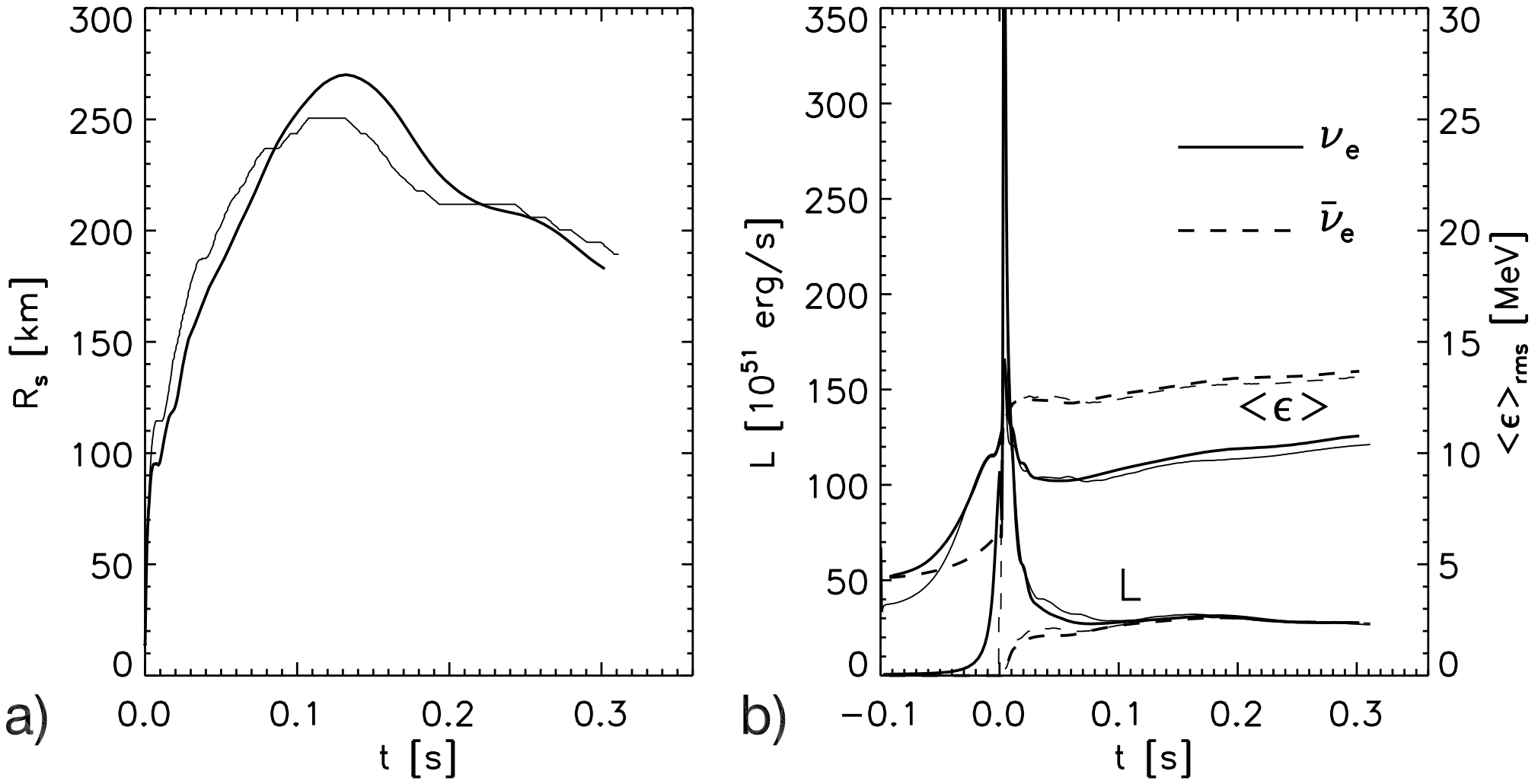

FIG. 5.—(*a*) Shock position as a function of time for model N13. The shock in VERTEX (*thin line*) propagates initially faster and nicely converges after its maximum expansion to the position of the shock in AGILE-BOLTZTRAN (*thick line*). (*b*) Neutrino luminosities and rms energies for model N13 are presented as functions of time. The values are sampled at a radius of 500 km in the comoving frame. The solid lines belong to electron neutrinos and the dashed lines to electron antineutrinos. The line width distinguishes between the results from AGILE-BOLTZTRAN and VERTEX in the same way as in (*a*). The luminosity peaks are nearly identical; the rms energies have the tendency to be larger in AGILE-BOLTZTRAN.

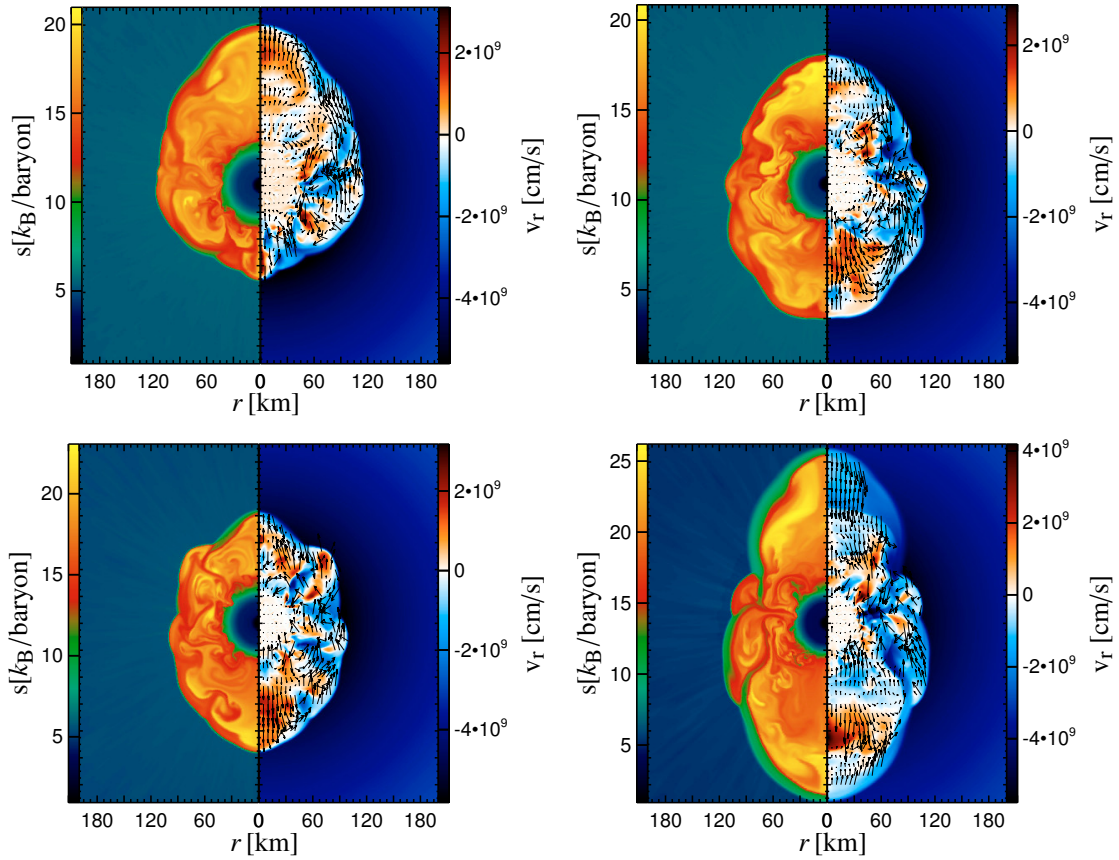

Fig. 3. Four representative snapshots from the 2D simulation with the L&S EoS at post-bounce times of 247 ms (*top left*), 255 ms (*top right*), 322 ms (*bottom left*), and 375 ms (*bottom right*). *The lefthand panel* of each figure shows color-coded the entropy distribution, *the righthand panel* the radial velocity component with white and whitish hues denoting matter at or near rest; black arrows in the *righthand panel* indicate the direction of the velocity field in the post-shock region (arrows were plotted only in regions where the absolute values of the velocities were less than 2×10^9 cm s^{-1}). The vertical axis is the symmetry axis of the 2D simulation. The plots visualize the accretion funnels and expansion flows in the SASI layer, but the chosen color maps are unable to resolve the convective shell inside the nascent neutron star.

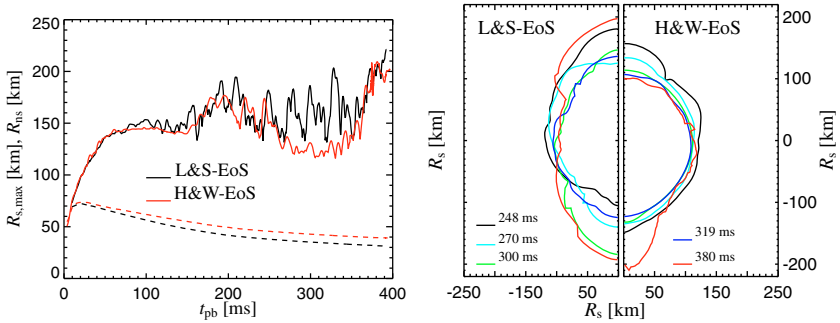

Fig. 4. *Left*: maximum shock radii (solid lines) and proto-neutron star radii (dashed lines) as functions of post-bounce time for the 2D simulations with different nuclear equations of state. The neutron star radii are determined as the locations where the rest-mass density is equal to 10^{11} g cm^{-3}. *Right*: shock contours at the different post-bounce times listed in the figure. The vertical axis of the plot is the symmetry axis of the simulation.

Marek *et al.*, Astron. Astrophys. 496 (2009) 475

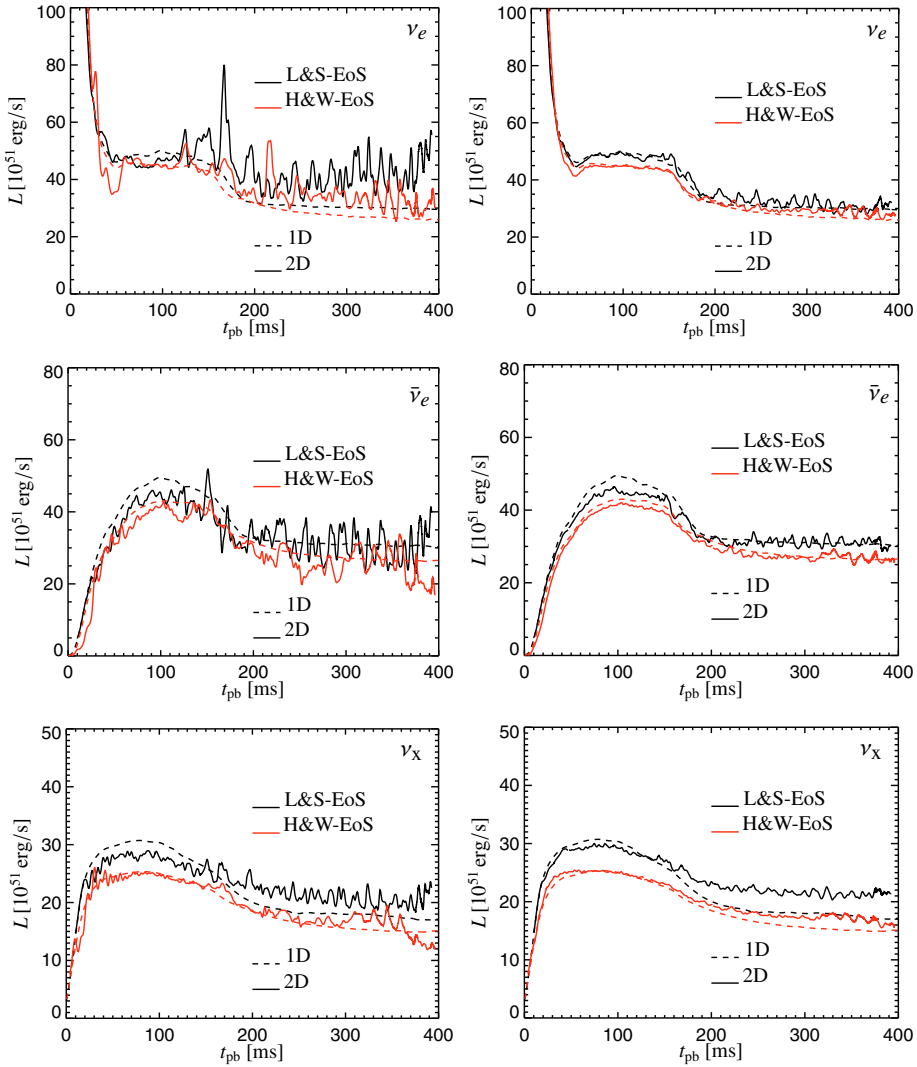

Fig. 6. Isotropic equivalent luminosities of electron neutrinos (*top*), electron antineutrinos (*middle*), and one kind of heavy-lepton neutrinos (ν_μ, $\bar{\nu}_\mu$, ν_τ, or $\bar{\nu}_\tau$; *bottom*) versus time after core bounce as measurable for a distant observer located along the polar axis of the 2D spherical coordinate grid (solid lines). The dashed lines display the radiated luminosities of the corresponding spherically symmetric (1D) simulations. The evaluation was performed at a radius of 400 km (from there the remaining gravitational redshifting to infinity is negligible) and the results are given for an observer at rest relative to the stellar center. While the left column shows the (isotropic equivalent) luminosities computed from the flux that is radiated away in an angular grid bin very close to the north pole, the right column displays the emitted (isotropic equivalent) luminosities when the neutrino fluxes are integrated over the whole northern hemisphere of the grid (see Eqs. (2) and (4), respectively).

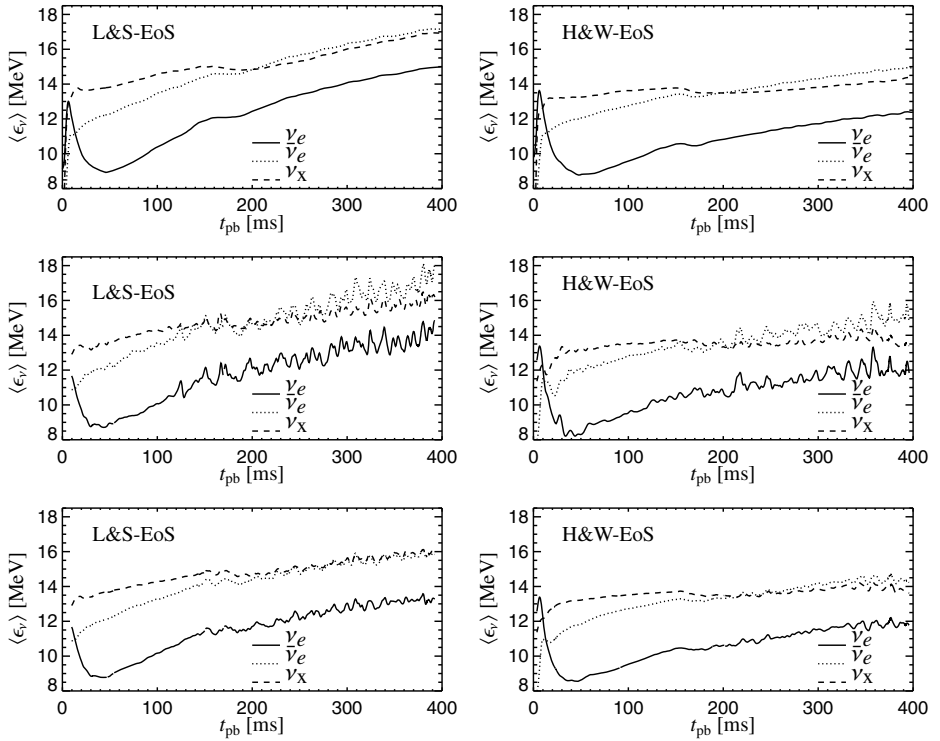

Fig. 7. Mean energies of radiated neutrinos as functions of post-bounce time for our 1D simulations (*top*) and 2D models (*middle* and *bottom*) with both equations of state (the lefthand panels are for the L&S EoS, the right ones for the H&W EoS). The displayed data are defined as ratios of the energy flux to the number flux and correspond to the luminosities plotted with dashed and solid lines in Fig. 6. *The panels in the middle* show results for a lateral grid zone near the north polar axis, the bottom panels provide results that are averaged over the whole northern hemisphere of the computational grid. In all cases the evaluation has been performed in the laboratory frame at a distance of 400 km from the stellar center.

$$\langle\omega_{\bar{\nu}_e}\rangle > \langle\omega_{\nu_x}\rangle \text{ but } \langle\omega_{\bar{\nu}_e}\rangle_{\mathrm{rms}} < \langle\omega_{\nu_x}\rangle_{\mathrm{rms}}$$

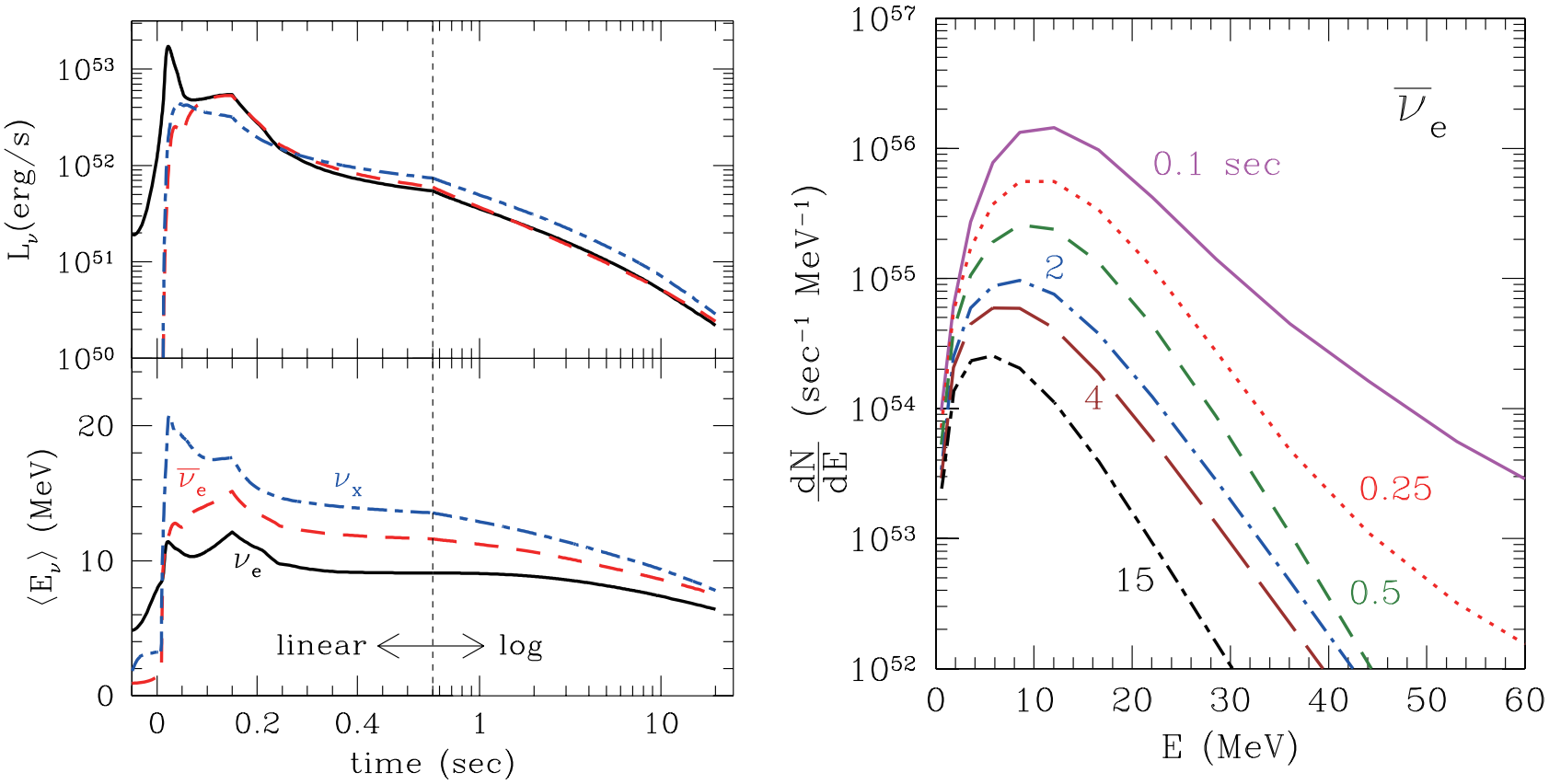

Figure 14. Time evolution of neutrino luminosity and average energy (left) and number spectrum of $\bar{\nu}_e$ (right) from νRHD and PNSC simulations with the interpolation (13) for the model with $(M_{\rm init}, Z, t_{\rm revive}) = (13\,M_\odot, 0.02, 100$ ms). In the left panel, solid, dashed, and dot-dashed lines represent ν_e, $\bar{\nu}_e$, and ν_x (dot-dashed lines), respectively. In the right panel, the lines correspond, from top to bottom, to 0.1, 0.25, 0.5, 2, 4, and 15 s after the bounce.

Supernova Neutrino Database: Nakazato *et al.*, 2013

`http://asphwww.ph.noda.tus.ac.jp/snn/`

三段階の超新星ニュートリノ

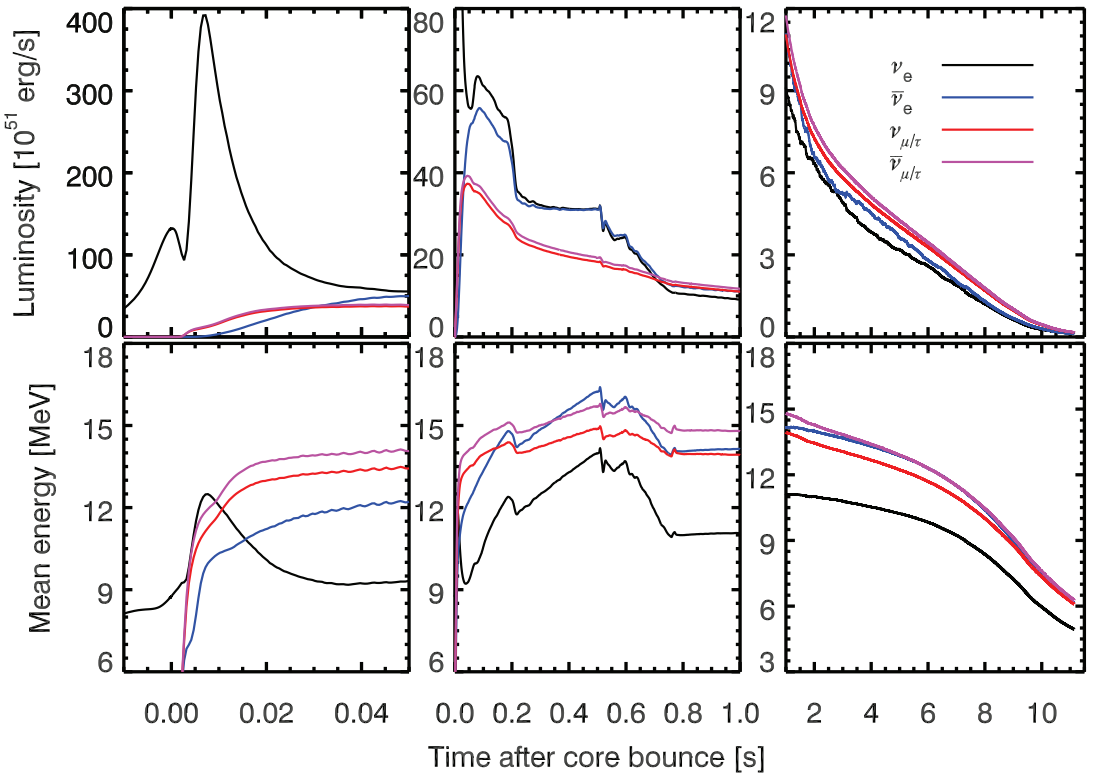

Fig. 8 Neutrino signal computed for the supernova explosion of a star of 27 $M_\odot$, which gives birth to a neutron star with 1.6 $M_\odot$. The *left panels* correspond to the shock-breakout phase, the *middle panels* to the post-bounce accretion phase including the transition to the proto-neutron star cooling phase, which is given in the *right panels*. The *upper panels* display the neutrino luminosities (ν_e black; $\bar{\nu}_e$: blue; one species of $\nu_{\mu,\tau}$: red; one species of $\bar{\nu}_{\mu,\tau}$: magenta), and the *lower panels* panels display the mean energies of the radiated neutrinos. In contrast to Fig. 7, the differences of heavy-lepton neutrinos and antineutrinos associated with weak-magnetism corrections of neutrino-nucleon scattering are shown. The slightly lower scattering opacity of $\bar{\nu}_{\mu,\tau}$ leads to slightly higher luminosities and higher mean energies (by ∼1 MeV) compared to those of $\nu_{\mu,\tau}$. The explosion sets in at 0.5 s after core bounce, but accretion onto the proto-neutron star ends only at about 0.75 s, which marks the onset of the cooling phase. (Figure courtesy of Robert Bollig)

Janka, arXiv:1702.08713

$$\sigma(\nu_x) > \sigma(\bar{\nu}_x)$$

Accretion phase:
ニュートリノ球の位置と降着物質の温度分布の関係から$\bar{\nu}_e$の平均エネルギーが高くなることもある。
(ν_xの化学平衡面から外での down scattering(ν e, ν N 散乱) も影響)

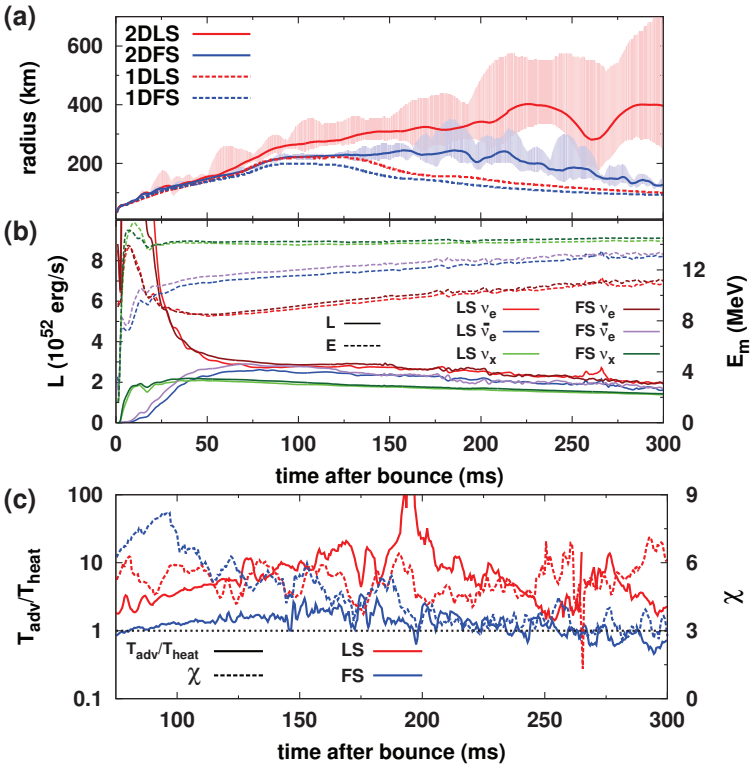

FIG. 1: (a) Shock radii as functions of time. The color-shaded regions show the ranges of the shock radii, red for the LS EOS and blue for the FS EOS. The solid lines are the angle-average values. For comparison, the corresponding results in spherical symmetry are displayed with dashed lines. (b) Time evolutions of the angle-integrated luminosities (L, solid lines) and the angle-averaged mean energies ($E_{\rm m}$, dashed lines) for different species of neutrinos. Both of them are measured at $r = 500$km. (c) The ratio of the advection to heating timescales ($T_{\rm adv}/T_{\rm heat}$, with solid lines) and the χ parameter (dashed lines). The dotted black line represents $T_{\rm adv}/T_{\rm heat} = 1$ and $\chi = 3$ for reference.

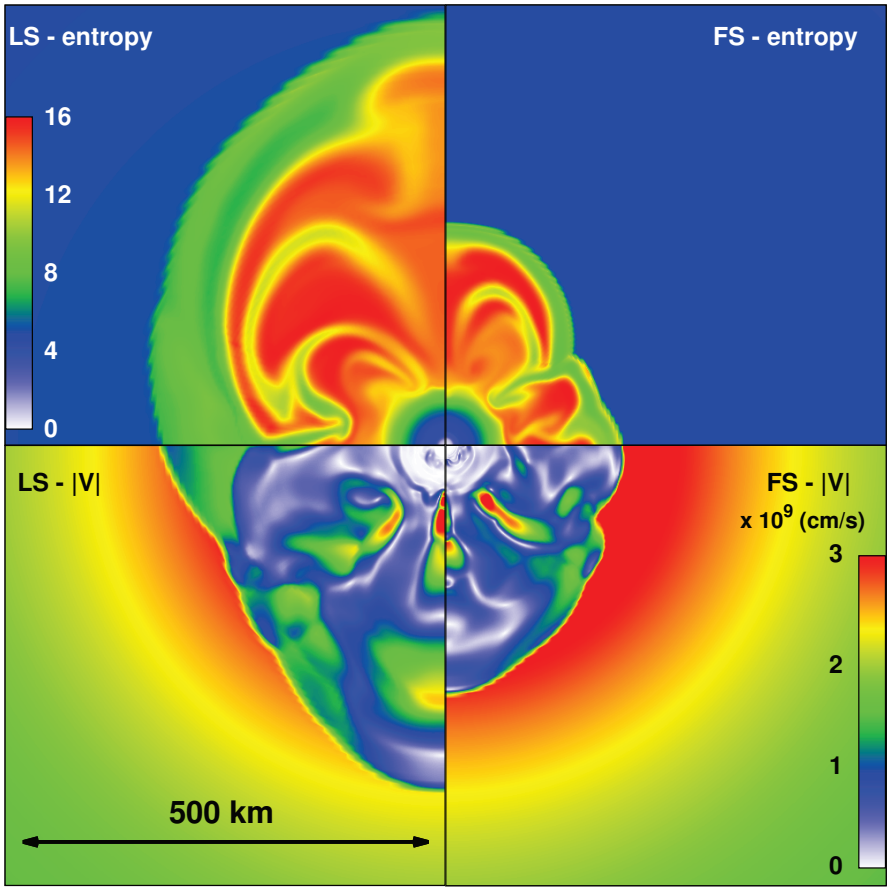

FIG. 2: Snapshots of entropy per baryon (upper) and fluid-speed (lower) at $t = 200$ms. Left and right panels are for the LS- and FS EOS, respectively.

Nagakura *et al.*, 2017 (Axisymmetric simulation with Boltzmann solver)
Towards full 3D Boltzmann solver

ニュートリノ振動

二世代ニュートリノ振動

異なる質量のニュートリノ (m_1, m_2) が存在し、その固有状態$|\nu_1\rangle$,$|\nu_2\rangle$と弱い相互作用の固有状態$|\nu_{\rm e}\rangle$,$|\nu_\mu\rangle$が一致しない時

$$
\begin{aligned}
U_{\alpha i} &\equiv \langle\nu_\alpha|\nu_i\rangle, \quad U = \begin{pmatrix} \cos\theta & \sin\theta \\ -\sin\theta & \cos\theta \end{pmatrix} \\
|\nu_\alpha\rangle &= \sum_i |\nu_i\rangle\langle\nu_i|\nu_\alpha\rangle = \sum_i U^\dagger_{i\alpha}|\nu_i\rangle = \sum_i U^*_{\alpha i}|\nu_i\rangle \\
|\nu_{\rm e}\rangle &= \cos\theta|\nu_1\rangle + \sin\theta|\nu_2\rangle \\
|\nu_\mu\rangle &= -\sin\theta|\nu_1\rangle + \cos\theta|\nu_2\rangle
\end{aligned}
$$

$i\frac{\partial}{\partial t}|\nu(t)\rangle = (H_0 + V)|\nu(t)\rangle$ から $\nu_\alpha(t) \equiv \langle\nu_\alpha|\nu(t)\rangle$ の時間発展方程式を導く

$$
\begin{aligned}
i\frac{\partial}{\partial t}|\nu(t)\rangle &= i\frac{\partial}{\partial t}\sum_\alpha |\nu_\alpha\rangle\langle\nu_\alpha|\nu(t)\rangle = i\sum_\alpha \frac{\partial\nu_\alpha(t)}{\partial t}|\nu_\alpha\rangle \\
H_0|\nu(t)\rangle &= \sum_{\alpha,\beta}\sum_{i,j} |\nu_\alpha\rangle\langle\nu_\alpha|\nu_i\rangle\langle\nu_i|H_0|\nu_j\rangle\langle\nu_j|\nu_\beta\rangle\langle\nu_\beta|\nu(t)\rangle \\
&= \sum_{\alpha,\beta}\sum_{i,j} |\nu_\alpha\rangle U_{\alpha i} E_i \delta_{ij} U^\dagger_{j\beta}\nu_\beta(t)
\end{aligned}
$$

$$V|\nu(t)\rangle = \sum_{\alpha,\beta} |\nu_\alpha\rangle\langle\nu_\alpha|V|\nu_\beta\rangle\langle\nu_\beta|\nu(t)\rangle = \sum_{\alpha,\beta} |\nu_\alpha\rangle V_\alpha \delta_{\alpha\beta}\nu_\beta(t)$$

なので、両辺の$|\nu_\alpha\rangle$の係数を比較して

$$i\frac{\partial \nu_\alpha(t)}{\partial t} = \sum_\beta \left(\sum_{ij} U_{\alpha i} E_i \delta_{ij} U^\dagger_{j\beta} + V_\alpha \delta_{\alpha\beta} \right) \nu_\beta(t)$$

行列形式

$$i\frac{\partial \vec{\nu}(t)}{\partial t} = H\vec{\nu}(t)$$

$$\vec{\nu}(t) \equiv \begin{pmatrix} \nu_{\mathrm{e}}(t) \\ \nu_\mu(t) \end{pmatrix}$$

$$H \equiv U \begin{pmatrix} E_1 & 0 \\ 0 & E_2 \end{pmatrix} U^\dagger + \begin{pmatrix} V_{\mathrm{e}} & 0 \\ 0 & V_\mu \end{pmatrix}$$

ニュートリノの質量が十分小さい近似では

$$E_i = \sqrt{p^2 + m_i^2} \sim p + \frac{m_i^2}{2p} \sim E + \frac{m_i^2}{2E}$$

$$\begin{pmatrix} E_1 & 0 \\ 0 & E_2 \end{pmatrix} = \left(E + \frac{m_1^2 + m_2^2}{4E} \right) I + \begin{pmatrix} -\frac{\Delta m^2}{4E} & 0 \\ 0 & \frac{\Delta m^2}{4E} \end{pmatrix}$$

$$I \equiv \begin{pmatrix} 1 & 0 \\ 0 & 1 \end{pmatrix}$$

一方、弱い相互作用に伴う有効ポテンシャル V は

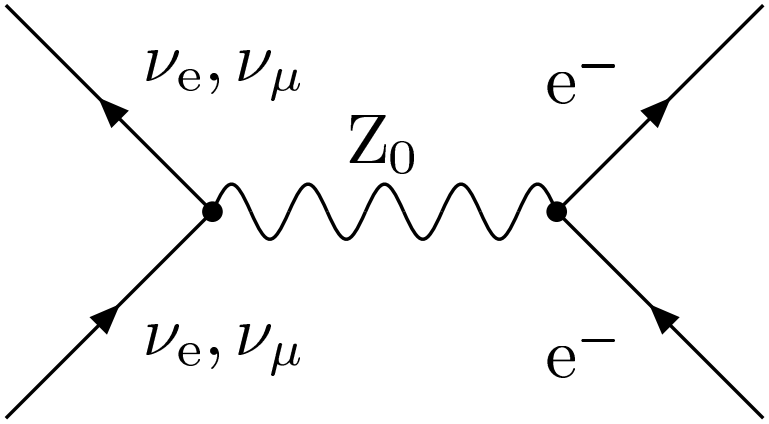

中性カレント V_{NC}

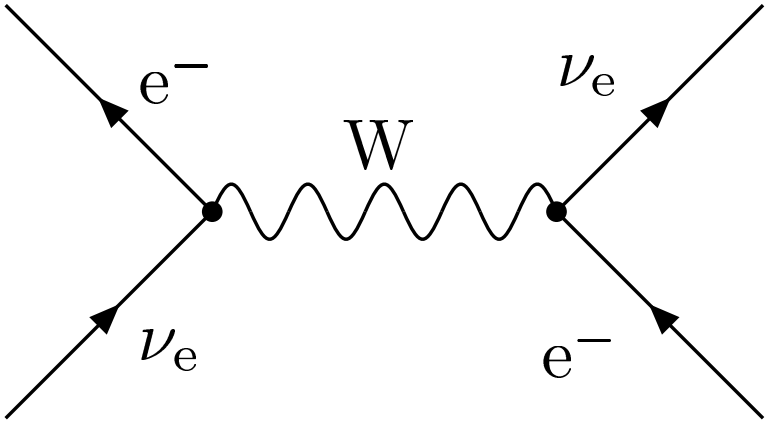

荷電カレント $V_{CC} = \sqrt{2} G_F n_e$

$V_e = V_{NC} + V_{CC}$、$V_\mu = V_{NC}$

$$U \begin{pmatrix} -1 & 0 \\ 0 & 1 \end{pmatrix} U^\dagger = \begin{pmatrix} -\cos 2\theta & \sin 2\theta \\ \sin 2\theta & \cos 2\theta \end{pmatrix}$$

などを使って、

$$H = \left(E + \frac{m_1^2 + m_2^2}{4E} + V_{NC} \right) I + H'$$

$$H' \equiv \begin{pmatrix} -\frac{\Delta m^2}{4E} \cos 2\theta + V_{CC} & \frac{\Delta m^2}{4E} \sin 2\theta \\ \frac{\Delta m^2}{4E} \sin 2\theta & \frac{\Delta m^2}{4E} \cos 2\theta \end{pmatrix}$$

単位行列 I に比例する項は、全体の位相に組み込まれるので，H' がニュートリノ振動を表す。

真空中のニュートリノ振動 ($V_{NC} = V_{CC} = 0$)

$$\vec{\nu}'(t) \equiv \exp\left\{i(E + \tfrac{m_1^2+m_2^2}{4E})t\right\}\vec{\nu}(t) \quad \text{とおくと}$$

$$i\frac{\partial\vec{\nu}'}{\partial t} = H'\vec{\nu}' \ , \quad H' = \frac{\Delta m^2}{4E}\begin{pmatrix} -\cos 2\theta & \sin 2\theta \\ \sin 2\theta & \cos 2\theta \end{pmatrix}, \quad U^\dagger H' U = \begin{pmatrix} -\frac{\Delta m^2}{4E} & 0 \\ 0 & \frac{\Delta m^2}{4E} \end{pmatrix}$$

$$\vec{\nu}'(t) = \mathrm{e}^{-iH't}\vec{\nu}'(0) = \left(\cos\left(\frac{\Delta m^2 t}{4E}\right) - i\sin\left(\frac{\Delta m^2 t}{4E}\right)H'\right)\vec{\nu}'(0)$$

$$\because \begin{pmatrix} -\cos 2\theta & \sin 2\theta \\ \sin 2\theta & \cos 2\theta \end{pmatrix}^2 = I$$

最初 ν_eだったとすると、$\vec{\nu}'(0) = \begin{pmatrix} 1 \\ 0 \end{pmatrix}$ とおいて、

$$\vec{\nu}'(t) = \begin{pmatrix} \nu_\mathrm{e}(t) \\ \nu_\mu(t) \end{pmatrix} = \begin{pmatrix} \cos\frac{\Delta m^2 t}{4E} + i\sin\frac{\Delta m^2 t}{4E}\cos 2\theta \\ -i\sin\frac{\Delta m^2 t}{4E}\sin 2\theta \end{pmatrix}$$

$$P(\nu_\mathrm{e} \to \nu_\mu) = |\nu_\mu(t)|^2 = \sin^2\frac{\Delta m^2 t}{4E}\sin^2 2\theta$$

$$P(\nu_\mathrm{e} \to \nu_\mathrm{e}) = |\nu_\mathrm{e}(t)|^2 = 1 - \sin^2\frac{\Delta m^2 t}{4E}\sin^2 2\theta = 1 - P(\nu_\mathrm{e} \to \nu_\mu)$$

Oscillation length $l_v \equiv \frac{4\pi E}{\Delta m^2} = 2.48\mathrm{m}\left(\frac{E}{1\mathrm{MeV}}\right)\left(\frac{\Delta m^2}{1\mathrm{eV}^2}\right)^{-1}$

$\sin^2 2\theta = 1$ ($\theta = \pi/4$)

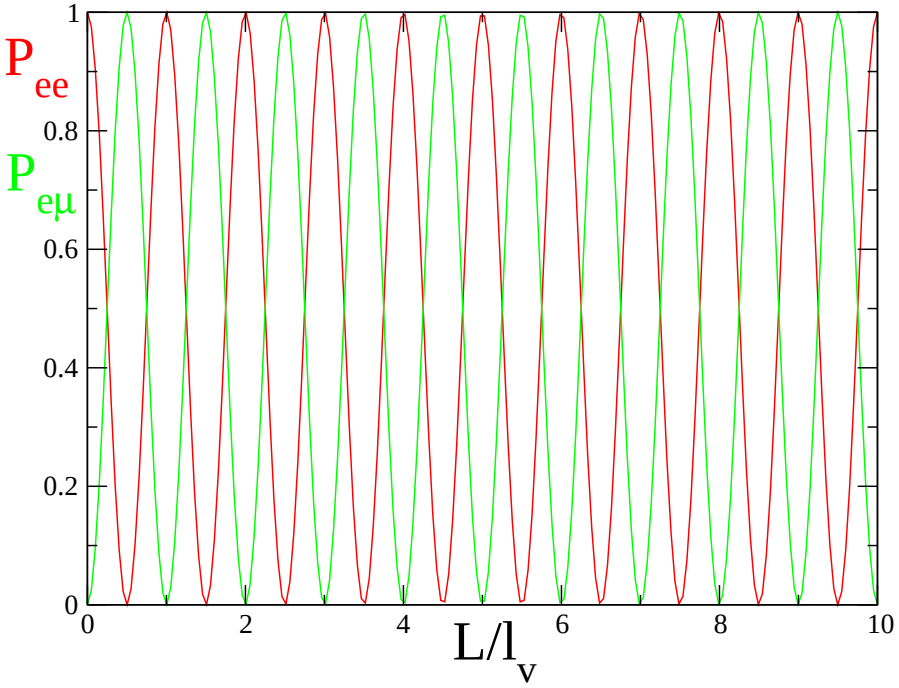

$\sin^2 2\theta = 0.1$

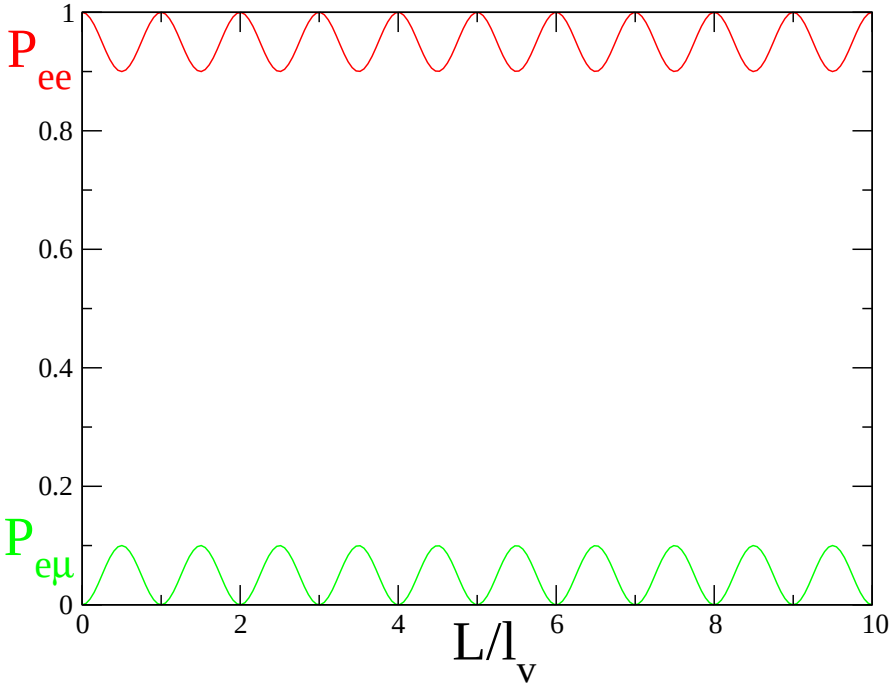

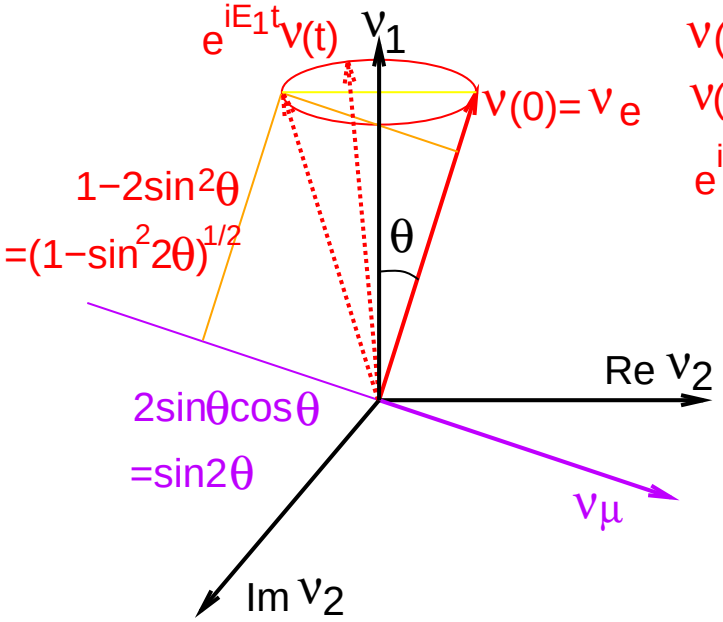

$$\nu_e = \cos\theta\,\nu_1 + \sin\theta\,\nu_2$$

$$\nu(0) = \nu_e$$

$$\nu(t) = \cos\theta\, e^{-iE_1 t}\nu_1 + \sin\theta\, e^{-iE_2 t}\nu_2$$

$$e^{iE_1 t}\nu(t) = \cos\theta\,\nu_1 + \sin\theta\, e^{i(E_1 - E_2)t}\nu_2$$

物質中でのニュートリノ振動 (MSW 効果)　$(V_{CC} \neq 0)$

H を対角化するするユニタリー行列 $U_m \neq U$

$$U_m^\dagger H U_m = \begin{pmatrix} E_{m1} & 0 \\ 0 & E_{m2} \end{pmatrix}$$

$$U_m = \begin{pmatrix} \cos\theta_m & \sin\theta_m \\ -\sin\theta_m & \cos\theta_m \end{pmatrix}$$

$$E_{m1,2} = E + \frac{m^2_{m1,2}}{2E} + V_{NC}$$

$$m^2_{m1,2} \equiv \left(\frac{m_1^2 + m_2^2}{2} + \frac{A}{2} \mp \frac{1}{2}\Delta m^2_m \right)$$

$$A \equiv 2EV_{CC} = 2\sqrt{2} G_F n_e E$$

$$\Delta m^2_m \equiv \sqrt{(A - \Delta m^2 \cos 2\theta)^2 + (\Delta m^2 \sin 2\theta)^2}$$

$$\tan 2\theta_m = \frac{\sin 2\theta}{\cos 2\theta - A/\Delta m^2}, \quad l_m \equiv l_v \frac{\Delta m^2}{\Delta m^2_m}$$

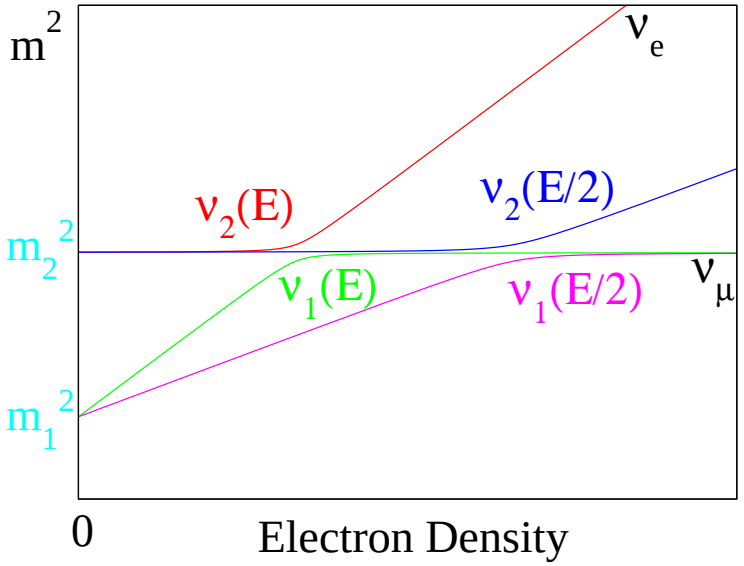

$$A, n_e \to 0 : m^2_{m1,2} \to m_1^2, m_2^2, \theta_m \to \theta$$

$$A, n_e \to \infty : m^2_{m1} \to m_1^2 \sin^2\theta + m_2^2 \cos^2\theta, \quad m^2_{m2} \to A \propto n_e$$

$$\tan 2\theta_m \to -0, \theta_m \to \frac{\pi}{2} \text{ (振動なし)}$$

共鳴 (resonance) 固有エネルギーの差が最小：$\cos 2\theta = A/\Delta m^2, \quad \theta_m = \pi/4$

$$n_{\rm e}({\rm res}) = \frac{\Delta m^2 \cos 2\theta}{2\sqrt{2} G_F E}, \quad \rho({\rm res}) = 1.3 \cdot 10^7 {\rm g/cm}^3 \left(\frac{Y_{\rm e}}{0.5}\right)^{-1} \left(\frac{\Delta m^2}{1{\rm eV}^2}\right) \left(\frac{E}{1{\rm MeV}}\right)^{-1} \cos 2\theta$$

Δm^2_m : 最小, $\quad \Delta m^2_m({\rm res}) = \Delta m^2 \sin 2\theta$

l_m : 最大, $\quad l_m({\rm res}) = l_v \dfrac{1}{\sin 2\theta}$

$$\rho_L = 4 \cdot 10\, {\rm g/cm}^3 \left(\frac{E}{10{\rm MeV}}\right)^{-1}, \ \rho_H = 3 \cdot 10^3\, {\rm g/cm}^3 \left(\frac{E}{10{\rm MeV}}\right)^{-1}$$

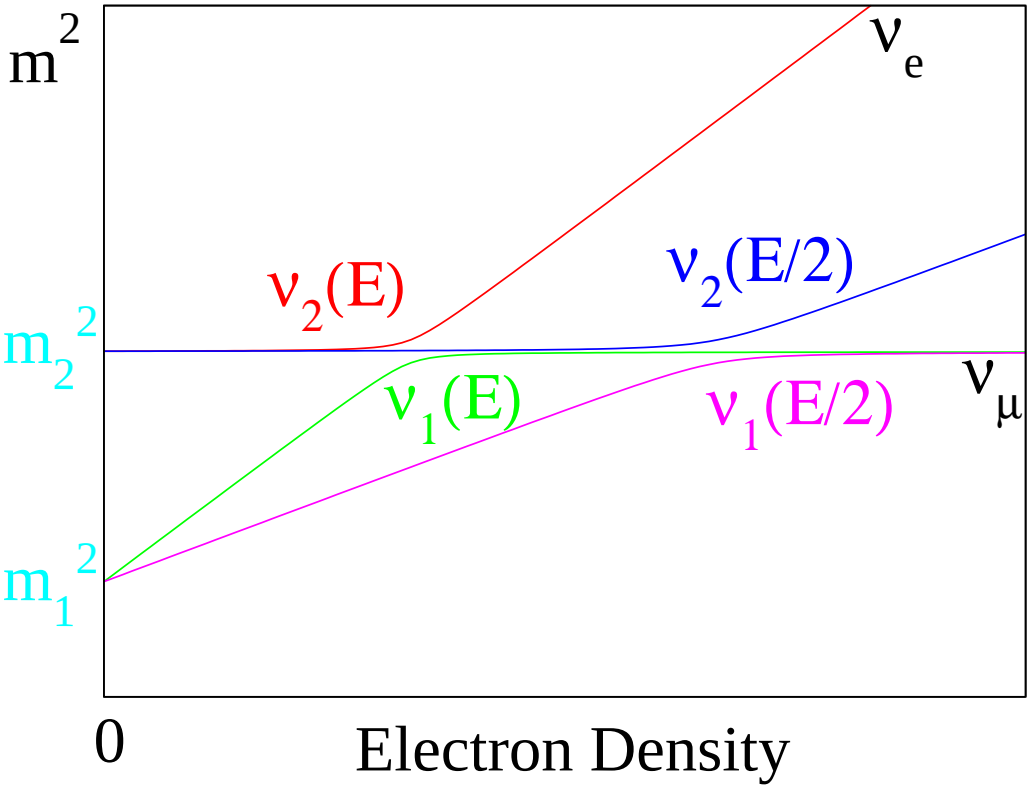

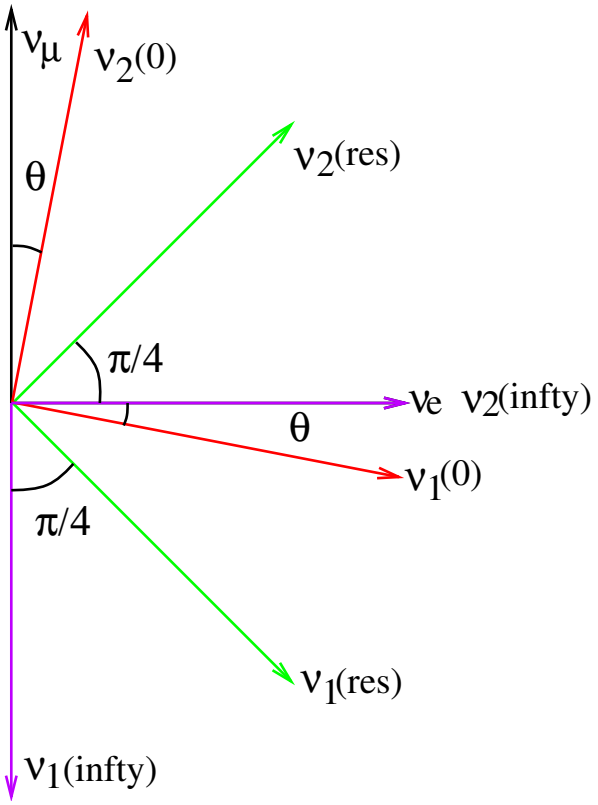

断熱条件: 物質密度が変化 ($\theta_m, \Delta m^2_m$ が変化) するとき

$$
\begin{aligned}
i\frac{\partial \vec{\nu}(t)}{\partial t} = H\vec{\nu}(t),\ \vec{\nu}(t) \equiv \begin{pmatrix} \nu_{\rm e}(t) \\ \nu_\mu(t) \end{pmatrix} = U_m \begin{pmatrix} \nu_{m1}(t) \\ \nu_{m2}(t) \end{pmatrix} = U_m \vec{\nu}_m(t) \text{ を代入} \\
i\frac{\partial \vec{\nu}_m(t)}{\partial t} &= \left(U_m^\dagger H U_m - iU_m^\dagger \frac{\partial U_m}{\partial t} \right) \vec{\nu}_m(t) = \begin{pmatrix} E_{m1} & -i\dot{\theta}_m \\ i\dot{\theta}_m & E_{m2} \end{pmatrix} \vec{\nu}_m(t) \\
&= \left(\frac{E_{m1}+E_{m2}}{2} + \begin{pmatrix} -\frac{\Delta m^2_m}{4E} & -i\dot{\theta}_m \\ i\dot{\theta}_m & \frac{\Delta m^2_m}{4E} \end{pmatrix} \right) \vec{\nu}_m(t)
\end{aligned}
$$

対角成分に比べて非対角成分が無視できる時、ν_{m1}、ν_{m2} はそれぞれの固有状態を保って進む (断熱的)。共鳴点で対角成分が最小になるので、共鳴点で $\frac{\Delta m^2_m}{2E} \gg |\dot{\theta}_m|$ であればよい。この断熱条件は

$$
\begin{aligned}
l_{\Delta m^2_m} &\equiv \frac{1}{\frac{1}{n_{\rm e}} \left| \frac{dn_{\rm e}}{dr} \right|} \frac{\sin 2\theta}{\cos 2\theta} : \quad \Delta m^2_m \text{の scale height} \\
l_\theta &\equiv \frac{l_m(\text{res})}{2\pi} = \frac{1}{\sin 2\theta} \frac{2E}{\Delta m^2} : \quad \text{振動のスケール}
\end{aligned}
$$

を使って $\gamma \equiv l_{\Delta m^2_m}/l_\theta \gg 1$ とも書ける。

断熱的でない場合、$P_{\rm jump} = \exp(-\frac{\pi}{2}\gamma)$ の確率で、$\nu_{m1} - \nu_{m2}$ 間の遷移が起こる。

3 世代のニュートリノ振動

$$
\begin{aligned}
i\frac{d}{dt}\begin{pmatrix}\nu_{\mathrm{e}}\\ \nu_{\mu}\\ \nu_{\tau}\end{pmatrix} &= \left(U_{\mathrm{MNS}}\begin{pmatrix}0 & 0 & 0\\ 0 & \Delta E_{21} & 0\\ 0 & 0 & \Delta E_{31}\end{pmatrix}U_{\mathrm{MNS}}^{\dagger}\right.\\
&\quad + \left.\begin{pmatrix}\sqrt{2}G_F n_{\mathrm{e}} & 0 & 0\\ 0 & 0 & 0\\ 0 & 0 & 0\end{pmatrix}\right)\begin{pmatrix}\nu_{\mathrm{e}}\\ \nu_{\mu}\\ \nu_{\tau}\end{pmatrix}
\end{aligned}
$$

$$
\begin{aligned}
&U_{\mathrm{MNS}}\\
&= \begin{pmatrix}1 & 0 & 0\\ 0 & c_{23} & s_{23}\\ 0 & -s_{23} & c_{23}\end{pmatrix}\begin{pmatrix}c_{13} & 0 & s_{13}e^{-i\phi}\\ 0 & 1 & 0\\ -s_{13}e^{i\phi} & 0 & c_{13}\end{pmatrix}\begin{pmatrix}c_{12} & s_{12} & 0\\ -s_{12} & c_{12} & 0\\ 0 & 0 & 1\end{pmatrix}\\
&= \begin{pmatrix}c_{12}c_{13} & s_{12}c_{13} & s_{13}e^{-i\phi}\\ -s_{12}c_{23}-c_{12}s_{23}s_{13}e^{i\phi} & c_{12}c_{23}-s_{12}s_{23}s_{13}e^{i\phi} & s_{23}c_{13}\\ s_{12}s_{23}-c_{12}c_{23}s_{13}e^{i\phi} & -c_{12}s_{23}-s_{12}c_{23}s_{13}e^{i\phi} & c_{23}c_{13}\end{pmatrix}
\end{aligned}
$$

$$\Delta E_{ij} \equiv \frac{\Delta m_{ij}^2}{2E}$$

$$s_{ij} \equiv \sin\theta_{ij},\ c_{ij} \equiv \cos\theta_{ij}$$

ニュートリノ振動パラメーターの測定

Table 14.1: The best-fit values and 3σ allowed ranges of the 3-neutrino oscillation parameters, derived from a global fit of the current neutrino oscillation data (from [60]) . For the Dirac phase δ we give the best fit value and the 2σ allowed ranges; at 3σ no physical values of δ are disfavored. The values (values in brackets) correspond to $m_1 < m_2 < m_3$ ($m_3 < m_1 < m_2$). The definition of Δm^2 used is: $\Delta m^2 = m_3^2 - (m_2^2 + m_1^2)/2$. Thus, $\Delta m^2 = \Delta m^2_{31} - \Delta m^2_{21}/2 > 0$, if $m_1 < m_2 < m_3$, and $\Delta m^2 = \Delta m^2_{32} + \Delta m^2_{21}/2 < 0$ for $m_3 < m_1 < m_2$.

Parameter	best-fit	3σ
Δm^2_{21} $[10^{-5}$ eV $^2]$	7.37	$6.93 - 7.97$
$\lvert\Delta m^2\rvert$ $[10^{-3}$ eV $^2]$	2.50 (2.46)	$2.37 - 2.63$ $(2.33 - 2.60)$
$\sin^2\theta_{12}$	0.297	$0.250 - 0.354$
$\sin^2\theta_{23}$, $\Delta m^2 > 0$	0.437	$0.379 - 0.616$
$\sin^2\theta_{23}$, $\Delta m^2 < 0$	0.569	$0.383 - 0.637$
$\sin^2\theta_{13}$, $\Delta m^2 > 0$	0.0214	$0.0185 - 0.0246$
$\sin^2\theta_{13}$, $\Delta m^2 < 0$	0.0218	$0.0186 - 0.0248$
δ/π	1.35 (1.32)	$(0.92 - 1.99)$ $((0.83 - 1.99))$

Particle Data 2016

超新星ニュートリノとニュートリノ振動

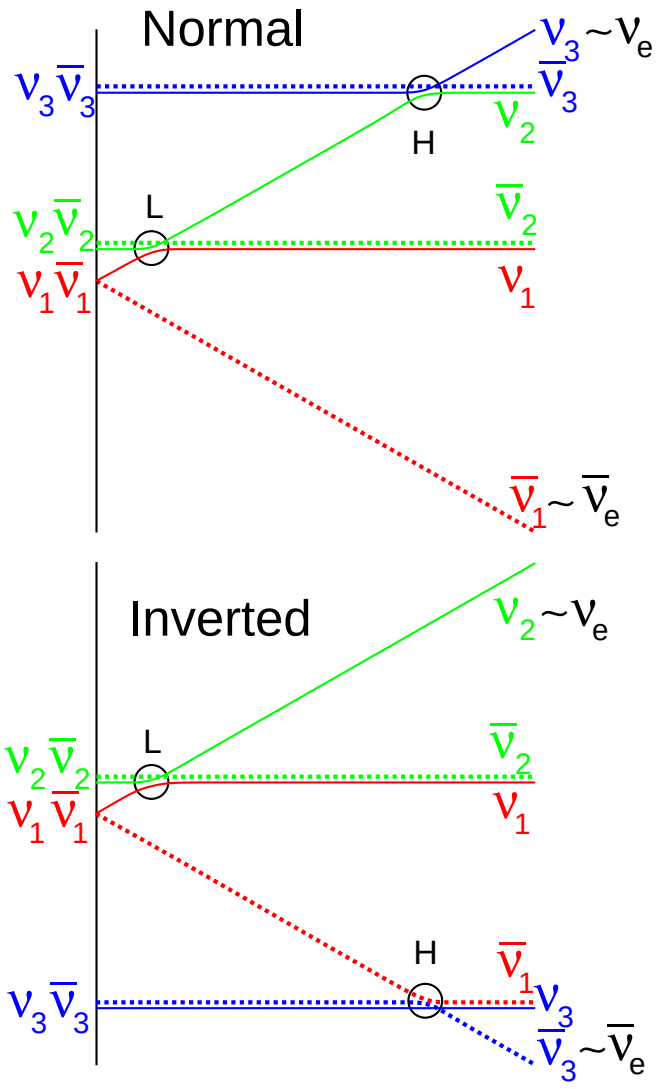

- H resonance: $\rho_H \sim 3 \cdot 10^3 \mathrm{g/cm}^3 \left(\frac{E}{10\mathrm{MeV}}\right)^{-1}$
  非断熱 (ONeMg core の ECSN 親星)
  断熱的 (Fe コアの CCSN 親星)
  $\Rightarrow \nu_e \Leftrightarrow \nu_3$ (normal), $\bar{\nu}_e \Leftrightarrow \bar{\nu}_3$ (inverted)
- L resonance: $\rho_L \sim 4 \cdot 10 \mathrm{g/cm}^3 \left(\frac{E}{10\mathrm{MeV}}\right)^{-1}$
  断熱的 $\nu_1 \Leftrightarrow \nu_2$

$$
\begin{aligned}
\phi_{\nu_x} &\equiv \frac{1}{4}(\phi_{\nu_\mu} + \phi_{\bar{\nu}_\mu} + \phi_{\nu_\tau} + \phi_{\bar{\nu}_\tau}) \\
\phi^{obs}_{\nu_e}(E) &= P(E)\phi^{SN}_{\nu_e}(E) + (1 - P(E))\phi^{SN}_{\nu_x}(E) \\
\phi^{obs}_{\bar{\nu}_e}(E) &= \bar{P}(E)\phi^{SN}_{\bar{\nu}_e}(E) + (1 - \bar{P}(E))\phi^{SN}_{\nu_x}(E) \\
4\phi^{obs}_{\nu_x}(E) &= (1 - P(E))\phi^{SN}_{\nu_e}(E) \\
&+ (2 + P(E) + \bar{P}(E))\phi^{SN}_{\nu_x}(E) \\
&+ (1 - \bar{P}(E))\phi^{SN}_{\bar{\nu}_e}(E)
\end{aligned}
$$

生き残り確率	P	$\bar{P}$
normal	$P_{\mathrm{H,jump}} \sin^2\theta_{12}$	$\cos^2\theta_{12} \sim 0.7$
inverted	$\sin^2\theta_{12} \sim 0.3$	$P_{\mathrm{H,jump}} \cos^2\theta_{12}$

$P_{\mathrm{H,jump}}$:H 共鳴での固有状態遷移確率 (断熱的なら 0)

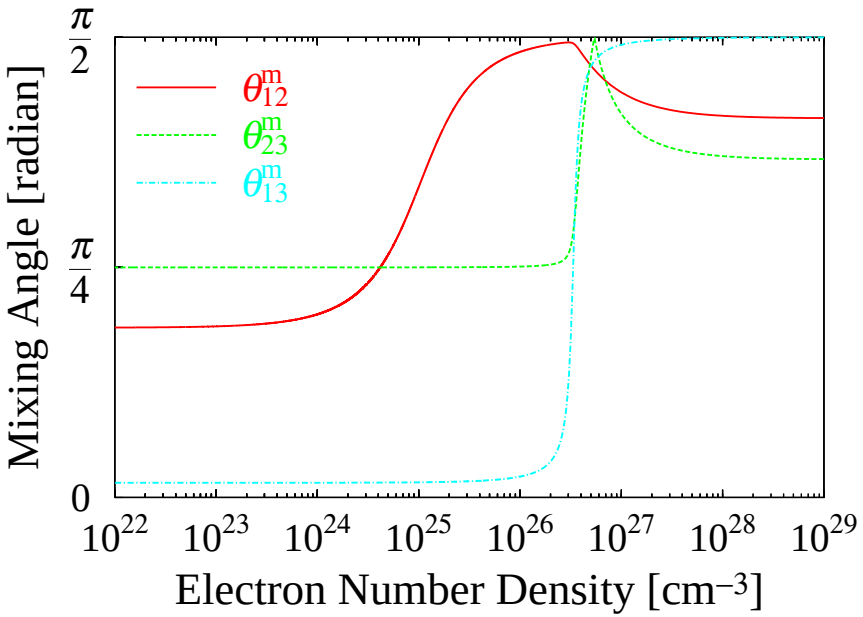

$E_\nu = 30\mathrm{MeV}$, normal hierarchy,
$\sin^2 2\theta_{13} = 10^{-2}$(未知だった頃の計算)

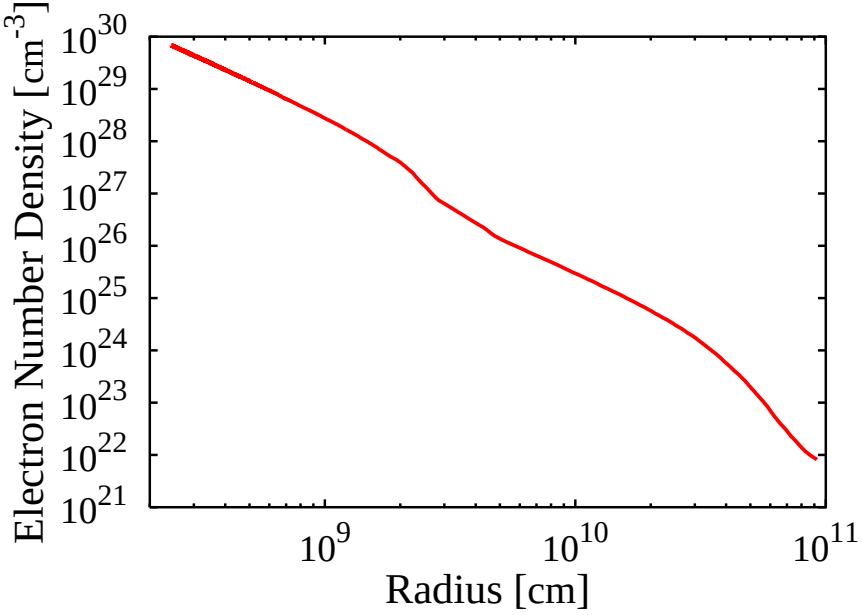

Progenitor $(15M_\odot)$ の密度分布 (Woosley and Weaver (1995))

$n_L \sim 3 \cdot 10^{24}\mathrm{cm}^{-3}$, $n_H \sim 3 \cdot 10^{26}\mathrm{cm}^{-3}$
共鳴領域で $\theta \sim \frac{\pi}{4}$
高密度領域では $\theta_{13}^m = \frac{\pi}{2}$
すなわち $\nu_\mathrm{e} = \nu_3$

衝撃波の伝播とニュートリノ振動

衝撃波面：密度不連続 $\Rightarrow$ ニュートリノ振動の断熱性の変化

衝撃波無し: H 共鳴も断熱的 $\rho_{\rm res} \propto \Delta m^2/E_\nu$

衝撃波の不連続面が、共鳴密度を通過中: H 共鳴は非断熱的

時間とともに、低密度・高エネルギーへ移動: 観測スペクトル $\Rightarrow$ 衝撃波の伝播の様子

衝撃波の形態によって、ニュートリノ振動によるスペクトル変形の様子が異なる。

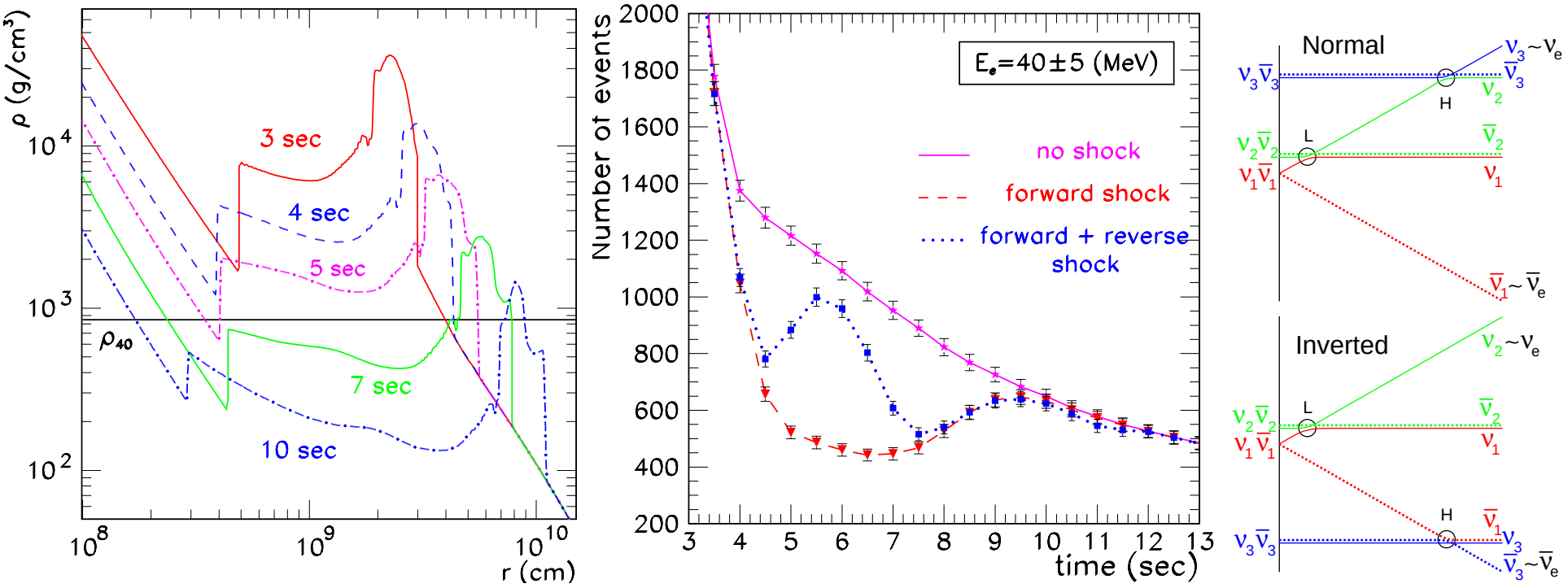

R. Tomas *et al.*, JCAP 0409 (2004) 015, IH, $\tan^2\theta_{13} = 10^{-2}$

衝撃波がないとき，断熱条件が満たされ$\bar{\nu}_{\rm e}$ の survival probability $\bar{P} = 0$ だったが、衝撃波が共鳴領域を通過するとき、断熱条件が破れ $\bar{P} > 0$ となり、平均エネルギーの高い$\bar{\nu}_x$ から$\bar{\nu}_{\rm e}$ への変換が減少。

衝撃波の伝播に伴い，非断熱的な衝撃波面の影響が低エネルギーから高エネルギーへ

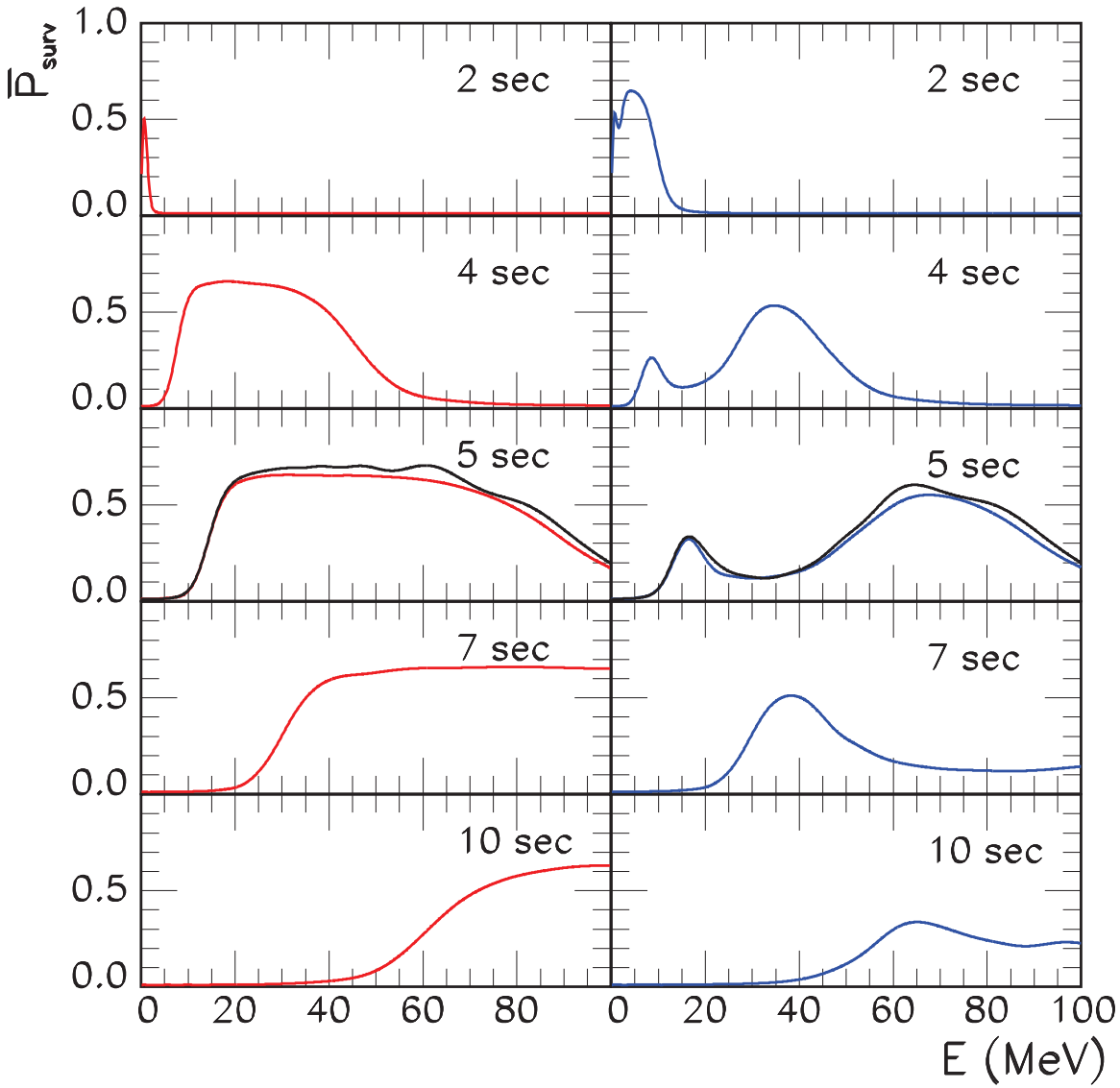

Figure 8. Survival probability $\bar{p}(E,t)$ as function of energy at different times averaging in energies with the energy resolution of Super-Kamiokande; for a profile with only a forward shock (left) and a profile with forward and reverse shock (right). At $t = 5$ s, we show $\bar{p}(E,t)$ including Earth matter effects for a zenith angle of the SN of 62° (black line).

R. Tomas *et al.*, JCAP 0409 (2004) 015, IH, $\tan^2\theta_{13} = 10^{-2}$

ONeMg Supernova (Lunardini, Müller and Janka, arXiv 0712.3000, θ_{13} 未知)

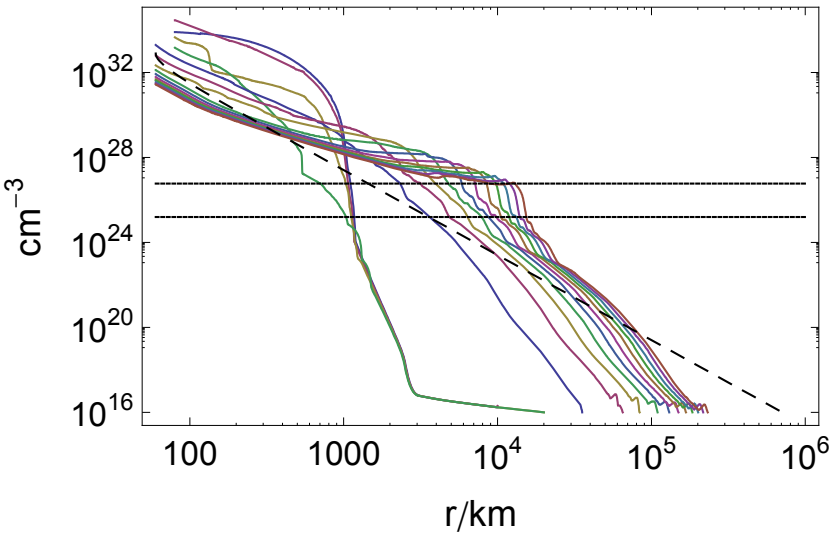

FIG. 1: Snapshots of the electron density profile at t = 0, 50, 100, ..., 700 ms (lines from top to bottom at their left end, except for the inverted curves for $t = 0$ and $t = 50$ ms). The positions of the supernova shock for $t \geq 200$ ms coincide essentially with the lower right footpoints of the profiles. For $t = 300$ ms we also plot the effective number density of neutrinos (dashed curve, see Eq. (4)), which is responsible for the effects of neutrino-neutrino forward scattering. The two horizontal lines represent the densities corresponding to the two MSW resonances for a neutrino of 20 MeV energy.

コア周辺に密度の急勾配分布をもつ ONeMg コアの爆発の場合，もともと非断熱的であった H-resonance が、衝撃波の通過後断熱的になることもありえる。
P_H: H-resonance の jump probability

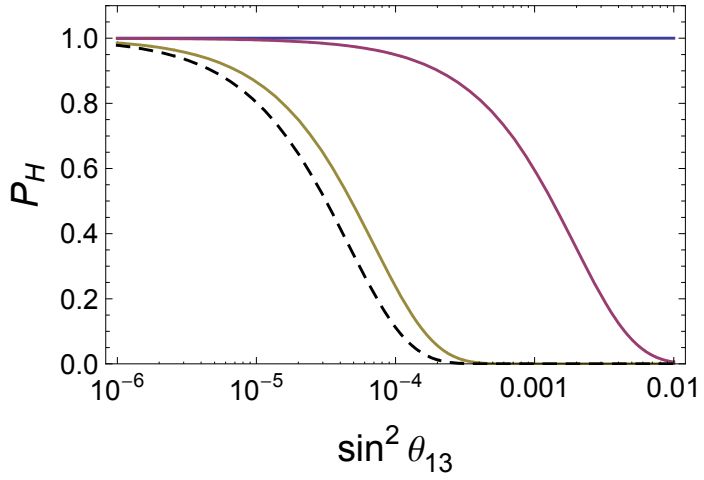

FIG. 3: The jumping probability P_H for $t = 60, 450, 700$ ms (solid curves, from upper to lower) as a function of $\sin^2\theta_{13}$ for energy $E = 20$ MeV. The dashed line shows the same probability for a Fe supernova with the parameters in ref. [3].

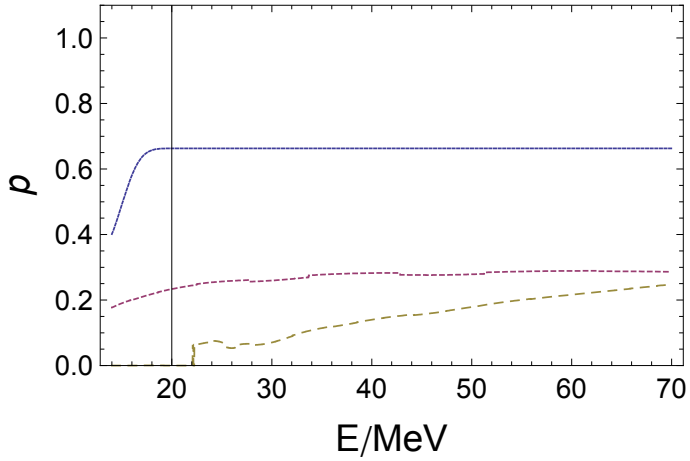

FIG. 4: The electron neutrino survival probability for t = 60, 450, 700 ms (solid, short dashed and long dashed respectively) and $\sin^2\theta_{13} = 6 \cdot 10^{-4}$. $p = 0$ for a Fe-core supernova over the same time interval.

衝撃波背面領域の乱流の影響：様々なスケールの密度揺らぎが質量固有状態の非断熱遷移を引き起こす

depolarization: survival prob. $P \to \frac{1}{2}$?

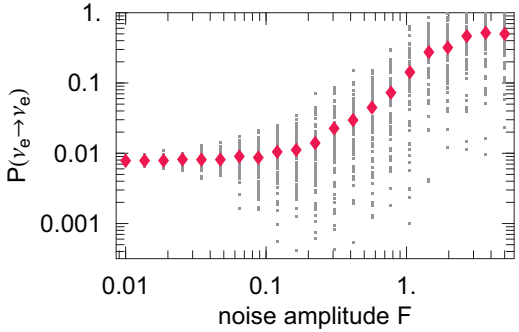

FIG. 1: The electron neutrino survival probability as a function of the noise amplitude F (see Eq. (3)). For each F, the calculation was repeated 66 times, with different random phases $\phi(k)$. The points indicate the results of individual runs, while the diamonds show the average values.

Friedland and Gruzinov, arXiv:0607244

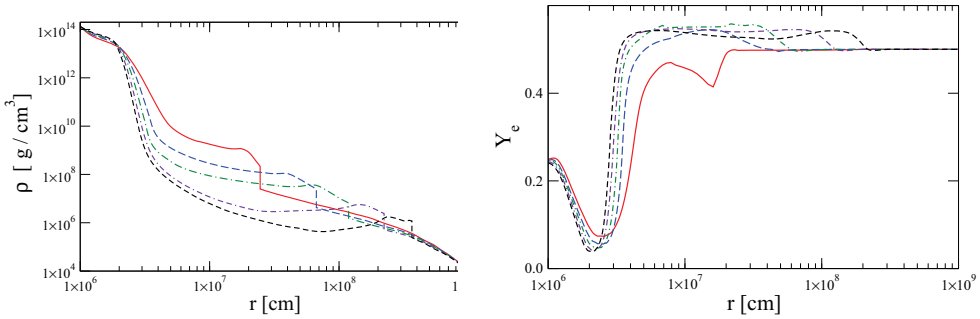

Figure 1. The density (left panel) and electron fraction (right panel) as a function of distance at various epochs post-bounce from the simulation by Fischer *et al.* [47] of the explosion of a $M = 10.8\ M_\odot$ progenitor. In both panels the epochs are $t = 0.3$ s (solid), $t = 0.4$ s (long dashed), $t = 0.5$ s (dash dot), $t = 0.6$ s (double dash dot), and $t = 0.7$ s (short dashed).

1D 流体計算結果+乱流モデル

Kneller and Reyes, arXiv:1702.06951

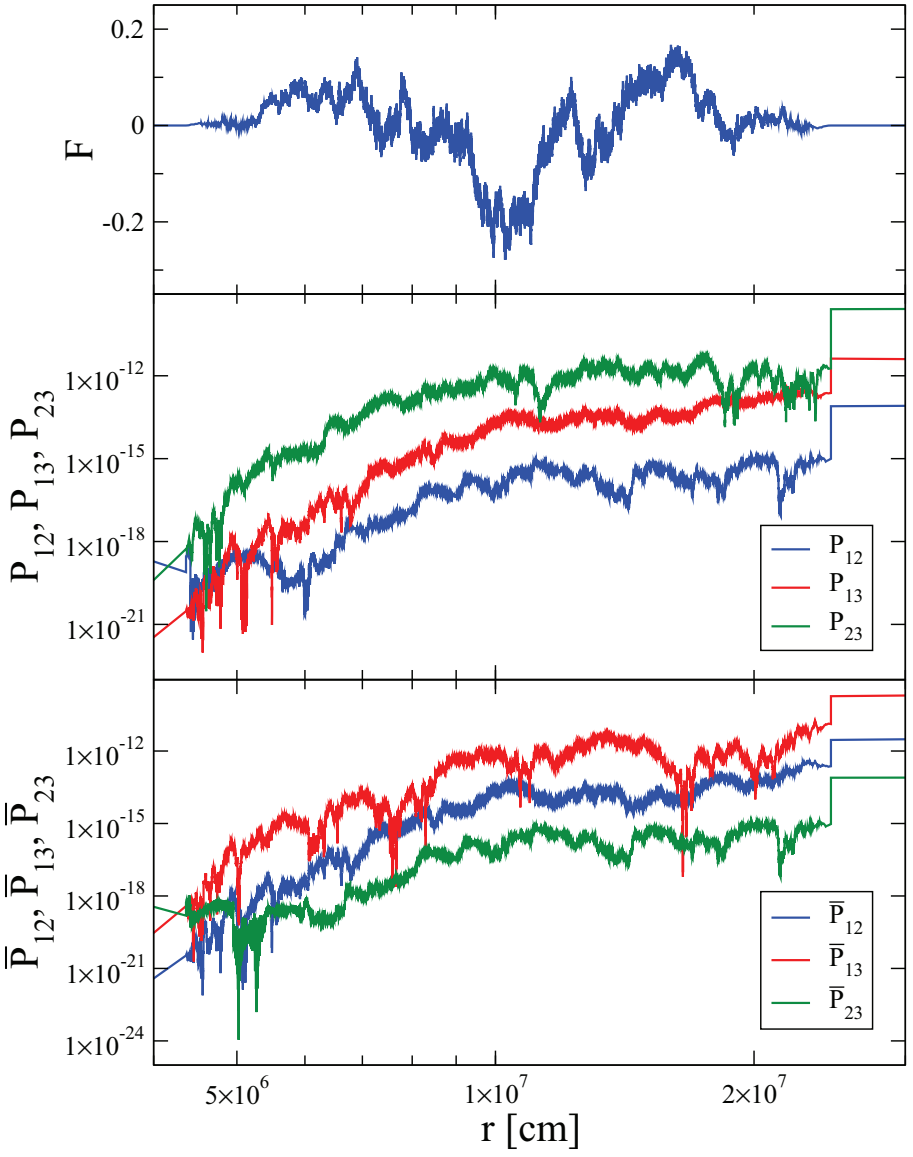

Figure 4. The random field F (top panel), the neutrino transition probabilities P_{12}, P_{13} and P_{23} (middle panel), and the antineutrino transition probabilities $\bar{P}_{12}$, $\bar{P}_{13}$ and $\bar{P}_{23}$ (bottom panel) as a function of distance r. For the lower two panels the colour coding is: P_{12} and $\bar{P}_{12}$ are blue, P_{13} and $\bar{P}_{13}$ are red, P_{23} and $\bar{P}_{23}$ are green. The density profile is the $t = 0.3$ s snapshot shown in figure (1).

遷移確率 $P \ll 1$: accretion phase は影響無

Collective Oscillation

参考： Mirizzi *et al.*, arXiv:1508.00785

$\nu\nu$ 反応による集団振動：超新星コア近傍では重要

$H_{\nu\nu} = \sqrt{2}G_F \int d^3p'(1-\hat{p}\cdot\hat{p}')(\rho_{p'} - \bar{\rho}_{p'})$ を追加

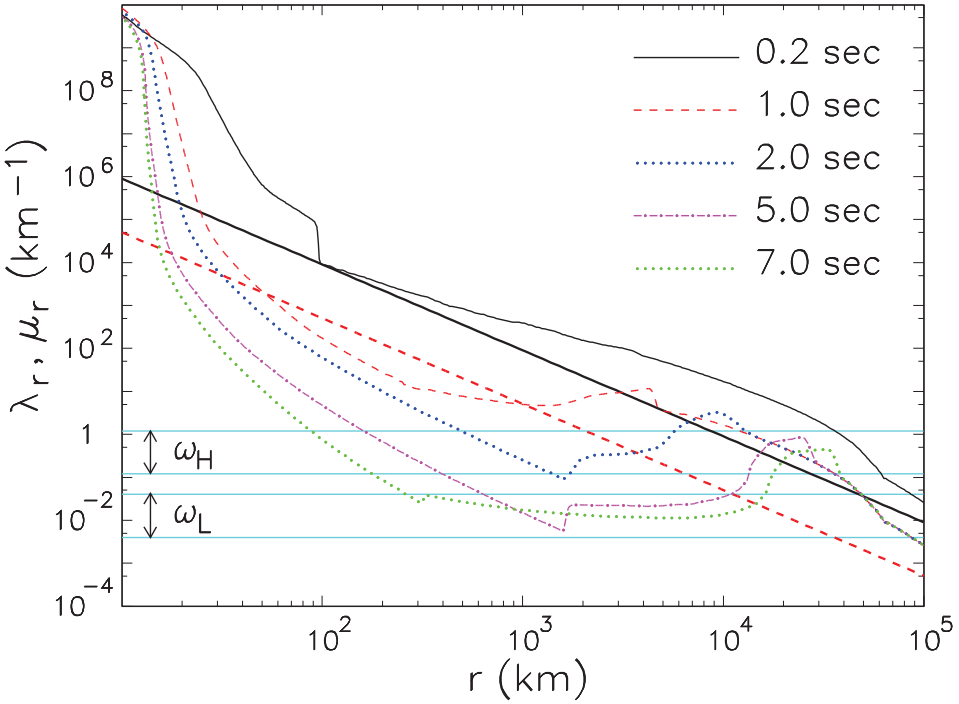

Fig. 22. – Snapshots of SN potentials for different post-bounce times (1.0 − 7.0 s) for a 27 $M_\odot$ SN progenitor (see Sec. **2**). The profile at 0.2 s is an illustrative case for a typical condition before shock revival. The matter potential λ_r is drawn with thin curves, while the neutrino potential μ_r with thick ones. The horizontal bands represent the vacuum oscillation frequencies relevant for the MSW resonant conversions associated with Δm^2 (ω_H) and δm^2 (ω_L), respectively (see the text for details).

Mirizzi *et al.*, arXiv1508.00785

$\omega \equiv \frac{\Delta m^2}{2E}$: 真空振動

$\lambda \equiv \sqrt{2}G_F(n_{e^-} - n_{e^+})$: 物質振動

$\mu \equiv \sqrt{2}G_F(n_{\bar{\nu}_e} - n_{\bar{\nu}_x})$

$= \frac{\sqrt{2}G_F}{4\pi r^2}\left(\frac{L_{\bar{\nu}_e}}{\langle E_{\bar{\nu}_e}\rangle} - \frac{L_{\bar{\nu}_x}}{\langle E_{\bar{\nu}_x}\rangle}\right)$: 集団振動

$t > 1\text{sec}$ $r < 10^3\text{km}$ で $n_\nu > n_e$

bulb model

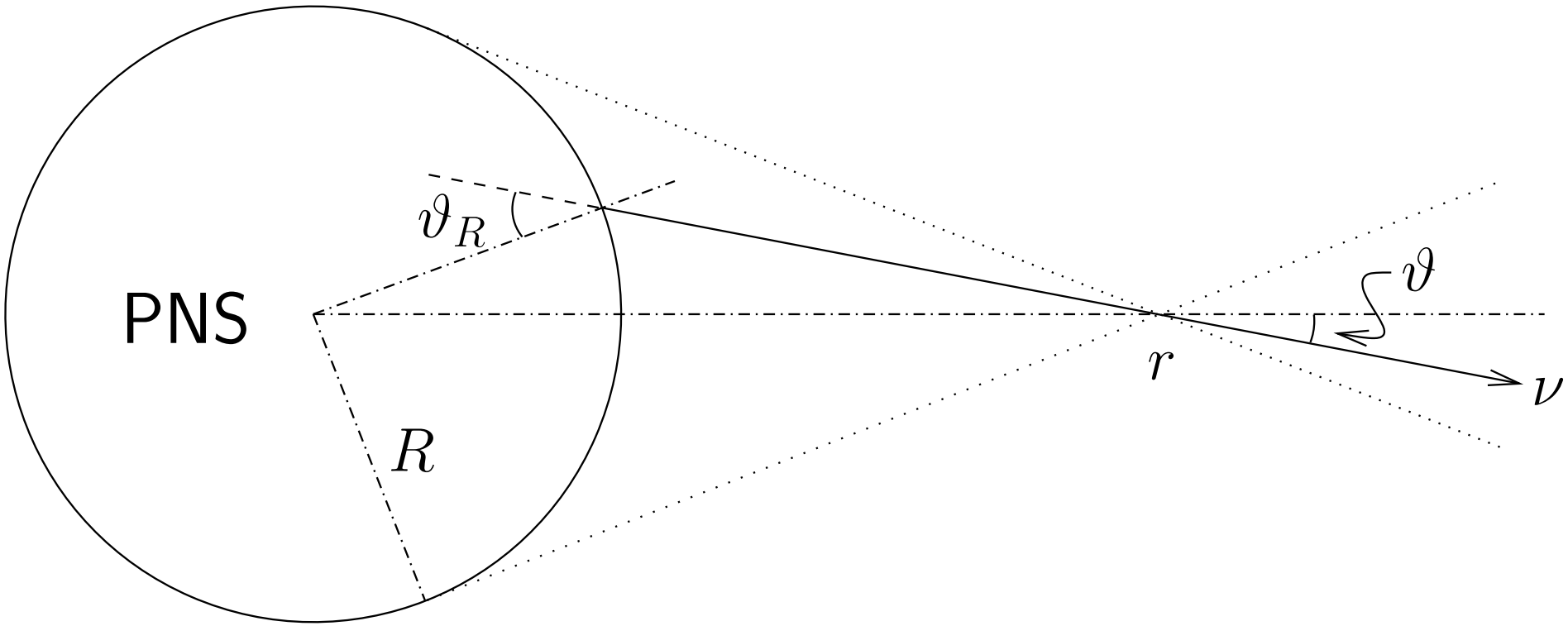

H. Duan *et al.*, arXiv:1001.2799

single-angle scheme (等方近似の式に帰結)
multi-angle scheme

accretion phase を想定した計算 ($F_{\nu_e} : F_{\bar{\nu}_e} : F_{\nu_x} = 2.4 : 1.6 : 1.0$)
Inverted Hierarchy: ν の spectral split ($E > E_{\rm split}$ が入れ替わる), $\bar{\nu}$ は、極低エネルギー以外が入れ替わる。normal hierarchy は集団振動なし。
近似的に L_e が保存するので、$\int_{E_{\rm split}}^{\infty}(F_{\nu_e} - F_{\nu_x})dE = \int_0^{\infty}(F_{\bar{\nu}_e} - F_{\bar{\nu}_x})dE$ が成り立つよう $E_{\rm split}$ が決まっている。

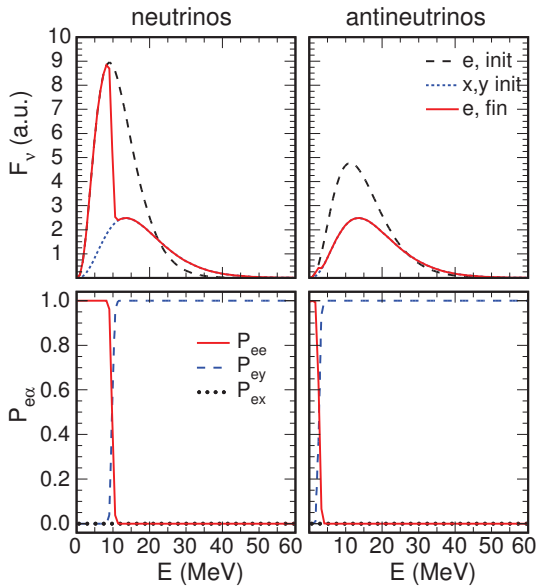

Fig. 26. – Case with $F^0_{\nu_e} : F^0_{\bar{\nu}_e} : F^0_{\nu_x} = 2.40 : 1.60 : 1.0$. Three-flavor evolution in the single-angle case and in inverted mass hierarchy for neutrinos (left panels) and antineutrinos (right panels). Upper panels: Initial energy spectra for ν_e (long-dashed curve) and $\nu_{x,y}$ (short-dashed curve) and for ν_e after collective oscillations (solid curve). Lower panels: Probabilities P_{ee} (solid red curve), P_{ey} (dashed blue curve), P_{ex} (dotted black curve). (Reprinted figure from [358]; copyright (2011) by the American Physical Society.)

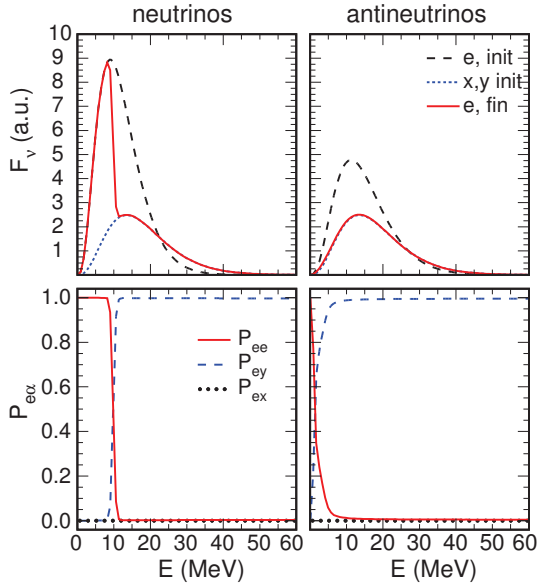

Fig. 27. – The same as Fig. 26 but in the multi-angle case. (Reprinted figure from [358]; cop (2011) by the American Physical Society.)

Mirizzi *et al.*, arXiv1508.00785, ここでは $\nu_{x,y} \equiv \cos\theta_{23}\nu_\mu \mp \sin\theta_{23}\nu_\tau$
single-angle と multi-angle は、差がない。
物質密度が高い ($\lambda > \mu$) と、集団振動が抑制されるが、物質密度が下がる late stage では、ニュートリノフラックスの差も小さくなってしまい、このような spectral split が実際に起こるか不明。

cooling phase を想定した計算 ($F_{\nu_e} : F_{\bar{\nu}_e} : F_{\nu_x} = 0.85 : 0.75 : 1.0$)
Normal でも Inverted Hierarchy でも: ν $\bar{\nu}$ とも、顕著ではないが multiple spectral split

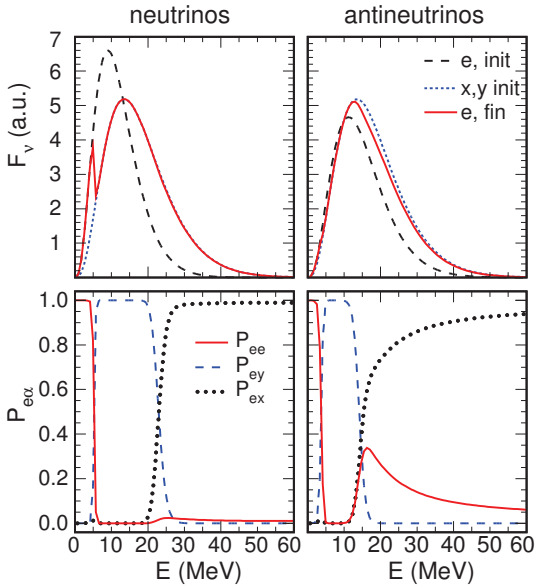

Fig. 28. – Case with $F^0_{\nu_e} : F^0_{\bar{\nu}_e} : F^0_{\nu_x} = 0.85 : 0.75 : 1.0$. Three-flavor evolution in the single-angle case and in inverted mass hierarchy for neutrinos (left panels) and antineutrinos (right panels). Upper panels: Initial energy spectra for ν_e (long-dashed curve) and $\nu_{x,y}$ (short-dashed curve) and for ν_e after collective oscillations (solid curve). Lower panels: Probabilities P_{ee} (solid red curve), P_{ey} (dashed blue curve), P_{ex} (dotted black curve). (Reprinted figure from [358]; copyright (2011) by the American Physical Society.)

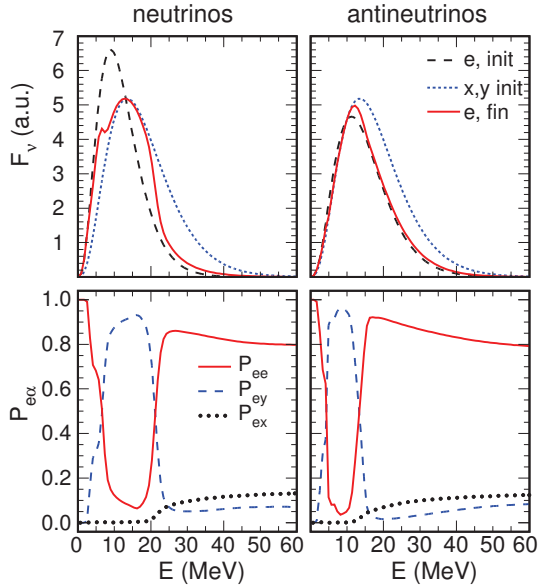

Fig. 29. – The same as Fig. 28 but in the multi-angle case. (Reprinted figure from [358
(2011) by the American Physical Society.)

Mirizzi *et al.*, arXiv1508.00785

single-angle と multi-angle は、差がある。

軸対称の仮定を外した計算 ($F_{\nu_e} : F_{\bar{\nu}_e} : F_{\nu_x} = 2.4 : 1.6 : 1.0$)
Normal でも Inverted Hierarchy でも、$\nu, \bar{\nu}$ ともにフレーバー変換あり。

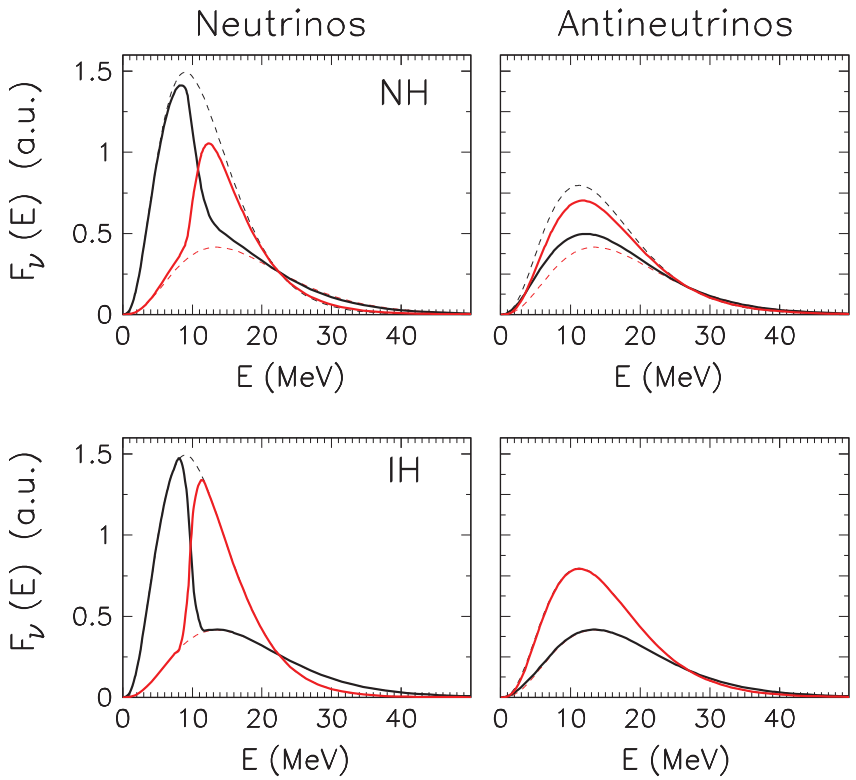

Fig. 30. – Multi-azimuthal-angle flavor evolution for ν's (left panel) and $\bar{\nu}$'s (right panel) in NH (upper panels) and IH (lower panels) for fluxes with an initial ordering $F^0_{\nu_e} : F^0_{\bar{\nu}_e} : F^0_{\nu_x} = 2.40 : 1.60 : 1.0$. Energy spectra for ν_e (black dashed curves) and ν_x (light dashed curves) in absence of flavor oscillations and for ν_e (black continuous curves) and ν_x (light continuous curves) after collective oscillations. (Reprinted figure from [367]; copyright (2014) by the American Physical Society.)

Mirizzi *et al.*, arXiv1508.00785
時間的，空間的な摂動による安定性解析が行われ，不安定なケースの存在が明らかになってきている。

Mirizzi らによるまとめ

TABLE II. – *Summary of multi-angle effects, 3ν effects and spectral splts for different SN neutrino fluxes, assuming sub-leading matter effects. The cases "accretion, $\lambda_r \ll \mu_r$" ("accretion, $\lambda_r \gg \mu_r$") stand for absence (presence) of multi-angle matter suppression effects.*

Initial spectral pattern	Multi-angle effects	δm^2-effects	Spectral splits
$F^0_{\nu_e} \gg F^0_{\nu_x} \gg F^0_{\bar{\nu}_e}$ (neutronization)	no	no	no
$F^0_{\nu_e} \gg F^0_{\bar{\nu}_e} \gg F^0_{\nu_x}$ (accretion, $\lambda_r \ll \mu_r$)	marginal	absent	robust
$F^0_{\nu_e} \gg F^0_{\bar{\nu}_e} \gg F^0_{\nu_x}$ (accretion, $\lambda_r \gg \mu_r$)	relevant	absent	no
$F^0_{\nu_x} \gtrsim F^0_{\nu_e} \gtrsim F^0_{\bar{\nu}_e}$ (cooling)	relevant	present/absent	smeared
$F^0_{\nu_e} \simeq F^0_{\nu_x} \simeq F^0_{\bar{\nu}_e}$ (cooling)	strong	present	washed-out

Mirizzi *et al.*, arXiv1508.00785

Volpe によるまとめ

Volpe, arXiv:1609.06747

球対称、定常 bulb モデルでは、spectral split が起こる。
物質効果 (multiangle にしたとき、角度ごとに物質の影響の受け方がことなる) により、集団振動が抑制される。
しかし非定常，非一様性を考慮すると、不安定性が成長する。

δ_{CP} の影響

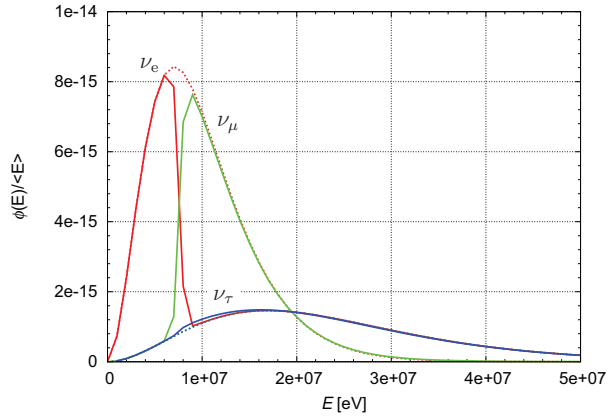

図 **4.5:** 質量階層：IH,CP 対称性が $\delta = 0$ のときの，終状態 ($r \sim 195$ km) のエネルギースペクトル．赤線が電子ニュートリノ，緑線がミューニュートリノ，青線がタウニュートリノを表している．点線が始状態，実線が終状態．

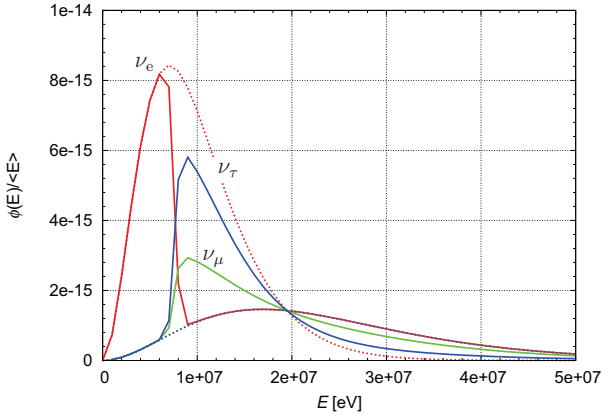

図 **4.7:** 質量階層：IH,CP 対称性が $\delta = 1.39\pi$ のときの，終状態 ($r \sim 195$ km) のエネルギースペクトル．赤線が電子ニュートリノ，緑線がミューニュートリノ，青線がタウニュートリノを表している．

藤井貴之修士論文 (東京理科大学) 2017

Fast conversion near the core

Dasgupta *et al.*, arXiv:1609.00528

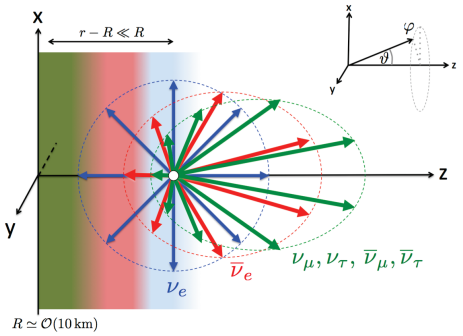

FIG. 1. Schematic geometry of the model and flavor-dependent zenith-angle distributions of neutrino fluxes. The 3 ellipses are schematic polar plots of the normalized angular distributions of the ν_e (blue), $\bar{\nu}_e$ (red), and ν_x (green) fluxes at the point where the arrows originate.

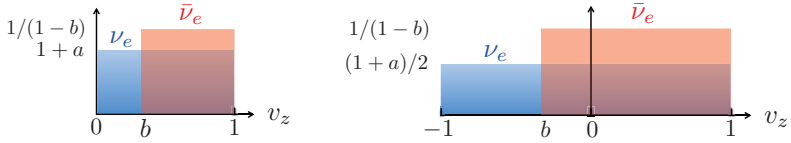

FIG. 2. Sketches of the schematic zenith angle distributions of ν_e (blue) and $\bar{\nu}_e$ (red), used for the calculations in this section. The left panel shows a spectrum that corresponds to Eq. (9) with no ingoing ν_e or $\bar{\nu}_e$, while the right panel shows a spectrum with ingoing ν_e and $\bar{\nu}_e$ as in Eq. (24). The ν_e and $\bar{\nu}_e$ have a flux ratio $1+a$, i.e., more ν_e than $\bar{\nu}_e$ when $a > 0$, and the $\bar{\nu}_e$ have a more forward-peaked distribution, controlled by the parameter b which we always choose to be larger than the $\min(v_z)$ for ν_e.

ニュートリノ球周辺 ($r \sim O(10)$km) を平面近似して線形解析

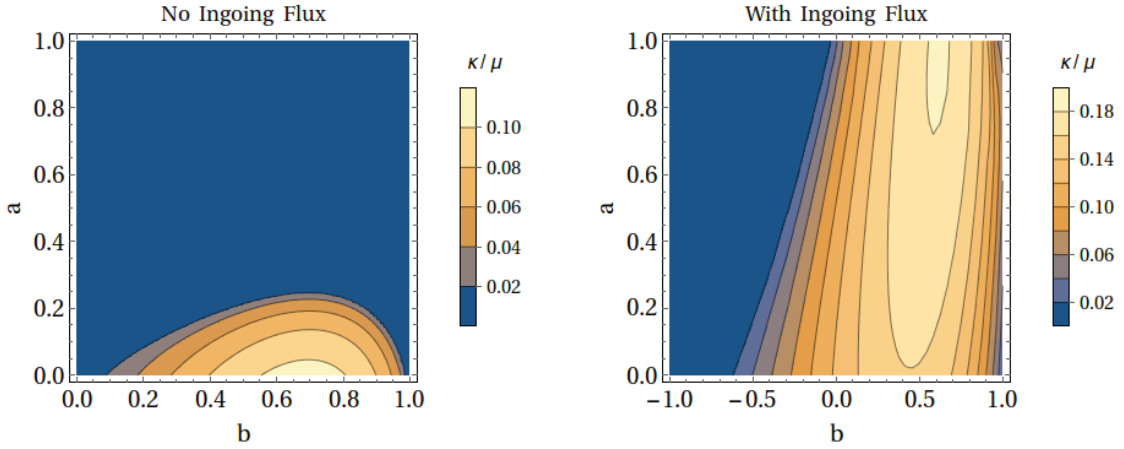

FIG. 4. Instability rates for different values of a and b, for evolution in time, without including inward going modes (left panel) and including inward going modes (right panel). These instabilities are azimuthally asymmetric, and we found no instabilities if the azimuthal symmetry were to be exact. There is no dependence on λ.

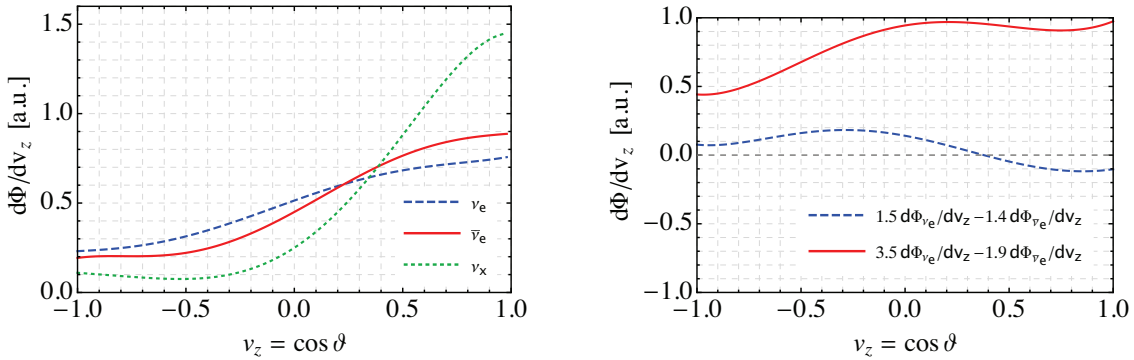

FIG. 6. Left panel: Normalized flavor-dependent zenith angle distributions of SN neutrinos from a one-dimensional SN model from the Garching group for a 25 $M_\odot$ progenitor at post-bounce time $t = 0.325\,\mathrm{s}$ and $r = 25\,\mathrm{km}$ [39]. Right panel: Difference of flux-weighted angular spectra of ν_e and $\bar{\nu}_e$, for two choices of flux ratios corresponding to small asymmetry (dashed line) and large asymmetry (solid line), respectively. Note that ν_x and $\bar{\nu}_x$ fluxes are equal and thus drop out.

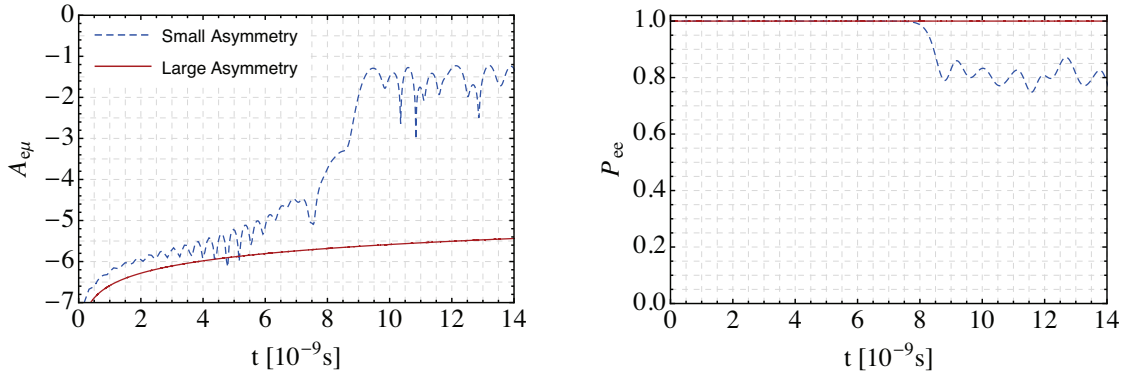

FIG. 7. Growth of fast instabilities for realistic SN neutrino angular distributions considered in this paper. The dashed and continuous curves correspond to the flux parameters with small and large lepton asymmetries, as may be expected due to LESA. While large asymmetries suppress the fast conversion, for smaller asymmetries there is $\simeq 20\%$ flavor conversion within a few nanoseconds. The growth of off-diagonal components is shown on the left panel, while the right panel shows the angle-integrated survival probability for $\bar{\nu}_e$.

ニュートリノ球近くで非常に速い (ns) 不安定性の成長: flavor equilibrium の可能性
ν_e, $\bar{\nu}_\mathrm{e}$ の角度分布の違い (大小関係の逆転) が重要、内向きフラックスも重要
(例えば，LESA の特定の方向: dipole に垂直方向)

Lepton-Emission Self-sustained Asymmetry: LESA

$F_{\nu_e} + F_{\bar{\nu}_e}$ はほぼ等方的でも、$F_{\nu_e} - F_{\bar{\nu}_e}$ が、方向によって数 10%異なる。(dipole 的)
PNS 内の convection や PNS への accretion が原因か?計算法に伴う人工的産物か？

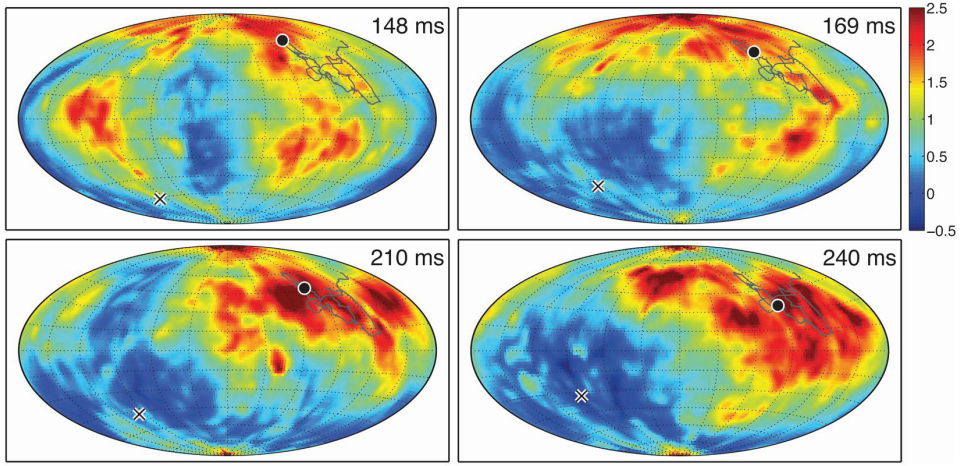

Fig. 6. – Time evolution of the lepton-number (ν_e minus $\bar{\nu}_e$) flux density normalized by the average value over all directions in a 3D core-collapse simulation of an 11.2 $M_\odot$ progenitor. The panels show "all-sky" images for the indicated post-bounce times. One can see the emergence of a clear dipole pattern with strong excess of the ν_e emission in one hemisphere and a reduced ν_e emission or even excess flux of $\bar{\nu}_e$ in the opposite hemisphere. This phenomenon has been found in all 3D simulations of the Garching group and was termed LESA for lepton-emission self-sustained asymmetry. The black dot marks the maximum of the dipole, the cross the anti-direction. The gray line indicates the path described by a slow drift of the dipole direction. (Image from Ref. [102]; copyright (2014) by the American Astronomical Society.)

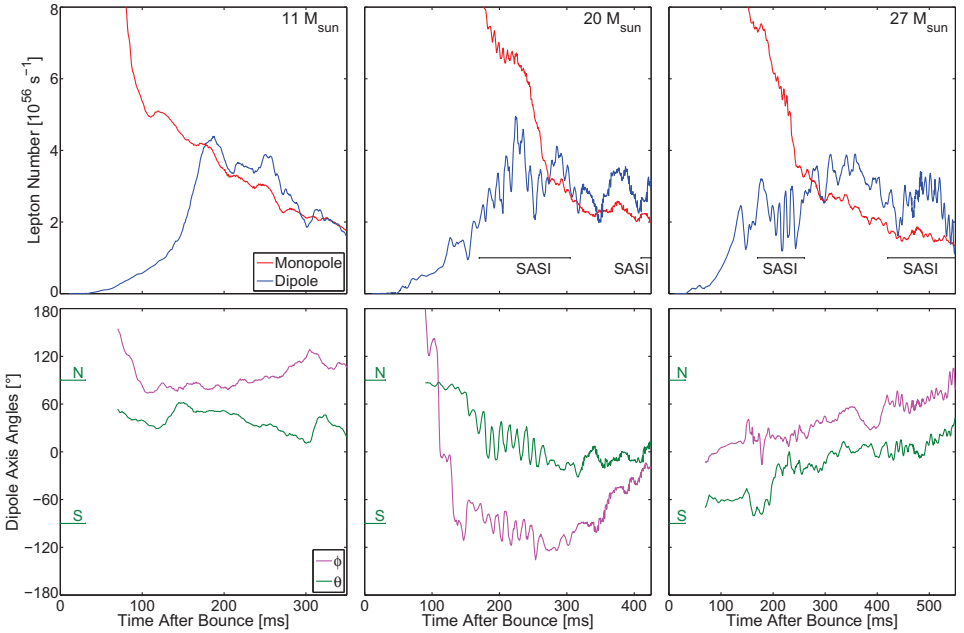

Fig. 7. – Post-bounce evolution of the lepton-number emission in 3D core-collapse simulations of 11.2 $M_\odot$ (*left*), 20 $M_\odot$ (*middle*) and 27 $M_\odot$ (*right*) progenitors. The upper panels show the monopole, i.e., the total lepton-number flux (red curve), and the dipole component (blue curve). The bottom panels display the polar angles θ and ϕ defining the dipole direction (i.e., the direction of the maximum excess of the ν_e emission relative to the $\bar{\nu}_e$ emission) in the polar coordinate grid of the star (north and south pole directions are indicated by "N" and "S", respectively). The monopole and dipole amplitudes $A_{\rm mon}$ and $A_{\rm dip}$ are normalized such that the lepton-number flux is given by $A_{\rm mon} + A_{\rm dip} \cos\vartheta$ in coordinates aligned with the dipole direction, if the flux distribution contains only monopole and dipole terms. (Image from Ref. [102]; copyright (2014) by the American Astronomical Society.)

LESA: Mirizzi *et al.*, arXiv1508.00785